A prospective and retrospective spatial sampling scheme to characterize geochemicals in a mine tailings area

Pravesh Debba

CSIR Built Environment
Logistics and Quantitative Methods (LQM)
South Africa

Presented at Nelson Mandela Metropolitan University 2009

Outline

Outline

Outline

Outline

Outline

The Problem

- Mine wastes contains high concentrations of metals.
- Metals — leached from mine wastes — then released to and contaminating nearby ecosystems.
- Geochemical characterization of mine waste impoundments – important for rehabilitation; remediation; protect the surrounding environment and ecosystems.
- Effective geochemical characterization – entails surface (to subsurface) sampling – labor or cost intensive.
- Metals in mine waste impoundments – hosted by acid-generating sulphide-rich minerals (pyrite, pyrrhotite), or adsorbed onto surfaces of weathering products of such sulphide-rich minerals.
- Such minerals are difficult to detect or identify by using current remote sensing techniques including multispectral or even hyperspectral data.

- Certain sulphide-rich minerals, particularly pyrite, weathers to a series of iron-bearing sulfates, hydroxides and oxides (shown by Swayze et al., 2000).
- Such secondary iron-bearing sulfates/hydroxides/oxides have diagnostic spectral features – enables their detection or identification with analytical techniques using hyperspectral data (Crowley et al., 2003).
- Debba et al. (2005) showed the potential of using hyperspectral data to estimate abundances of spectrally similar iron-bearing sulfates/hydroxides/oxides.
- Kemper & Sommer (2002) showed that heavy metal contamination in soils can be quantified using reflectance spectroscopy.

- Remote sensing provides an indirect tool for surface characterization of mine waste impoundments with oxidizing sulphide-rich materials; namely, for mapping spatial distributions of secondary iron-bearing sulfates/hydroxides/oxides and heavy metals.
- Hence, given a model of spatial distribution of secondary iron-bearing oxides/hydroxides, the problem is how to design a sampling scheme that would adequately capture the spatial distribution of certain groups of metals.
- Adaptation to Diggle & Lophaven (2006) retrospective sampling design — sequentially removes, from a sampling design, samples that contribute least to a Bayesian prediction of a response — not an optimal design.
- A prospective sampling scheme is derived for nearby unsampled areas based on the variogram model of the adjacent sampled area.

Study Area

- The present case study area is in the Recsk-Lahóca copper mining area in Hungary. The Recsk-Lahóca mining area is situated in the Mátra Mountains, about 110 km northeast of Budapest, Hungary.
- The Lahóca hill was mined for copper between 1852 and 1979.
- Mining of ore deposits in the Recsk-Lahóca area resulted in the exposure of sulphide bearing-rocks to surface water and atmospheric oxygen, which accelerate oxidation, leaching and release of metals and acidity.
- This study pertains to the tailings dumps northwest of Lahóca mine, which consist actually of two dumps referred to as "East Tails" and "West Tails".

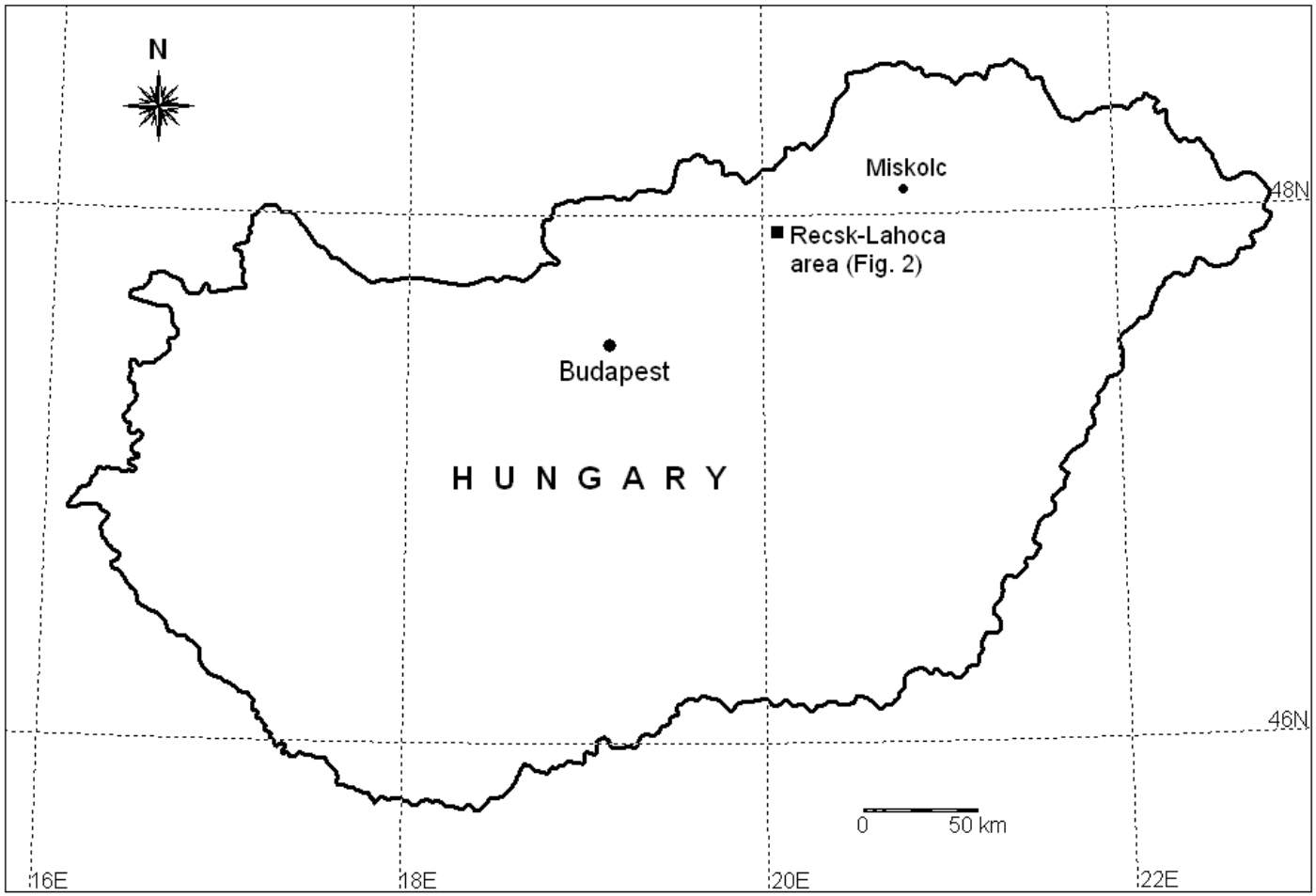

Figure: Study area: Recsk: Hungary.

The Data – Hyperspectral

- A subset of the Digital Airborne Imaging Spectrometer (DAIS-7915) is used.
- The resulting data is a 79 channel hyperspectral image, acquired over the Recsk. DAIS-7915 is a whisk broom sensor, covering a spectral range from visible (0.4 μm) to thermal infrared (12.3 μm) at variable spatial resolution from 3–20 m depending on the carrier aircraft altitude.
- Not all 79 channels were useful as many channels were too noisy and could not be corrected efficiently. Fortunately, the first 32 channels, spectral range 406-1035 nm, where iron-bearing oxides/hydroxides/sulphates have diagnostic features were found useful for this study.
- Samples from the tailings – collected shortly after collection of the DAIS hyperspectral data.

The Data – Field

- 53 samples were collected in the East Tails and 44 in the West tails – 10m$\times$10m grid points.
- Concentrations of As, Cd, Cu, Fe, Mn, Ni, Pb, Sb and Zn in the decomposed samples were determined using the ICP-AES analyzer.

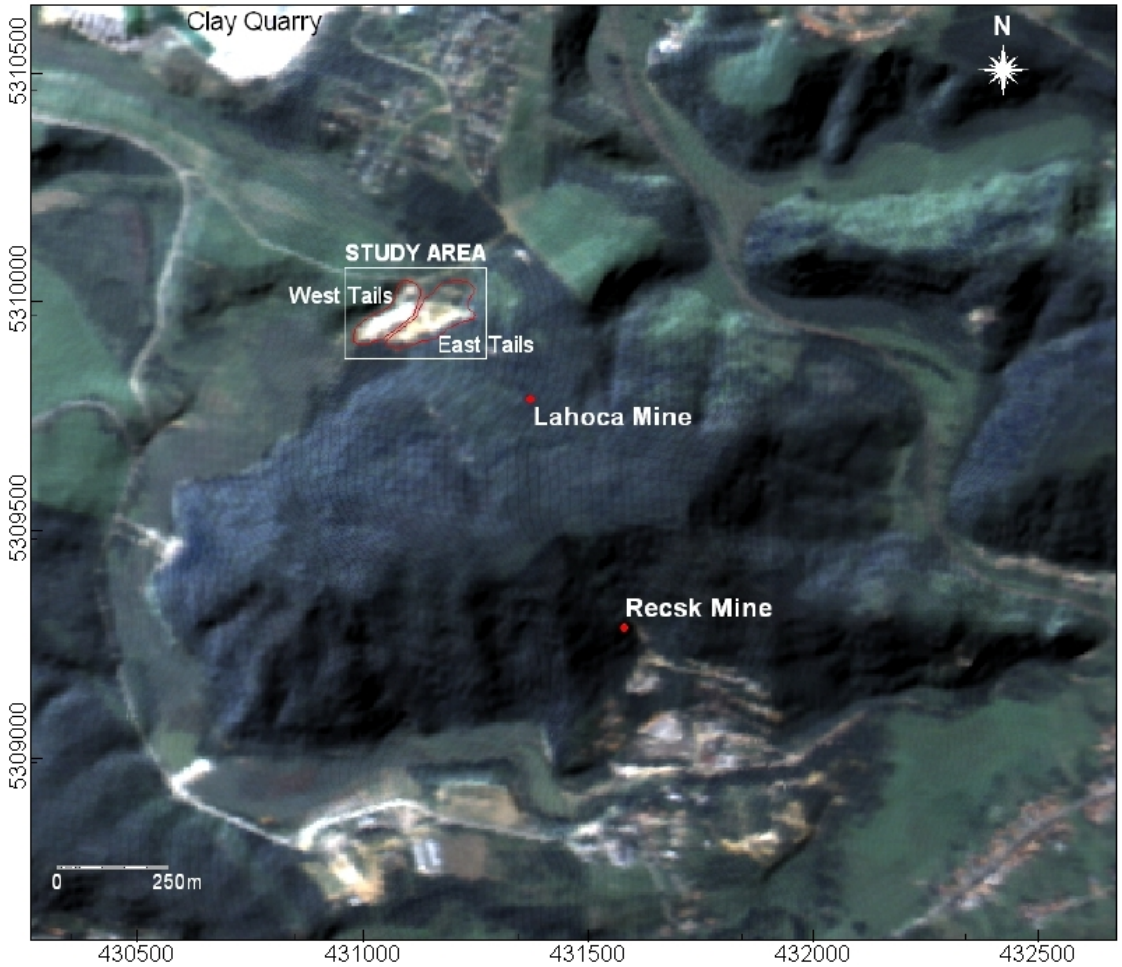

Figure: The Recsk-Lahóca area shown in pseudo-natural color composite image using DAIS data (red = ch10, green = ch5, blue = ch1) fused with a digital elevation model. Map coordinates are in meters (UTM projection, zone 34N).

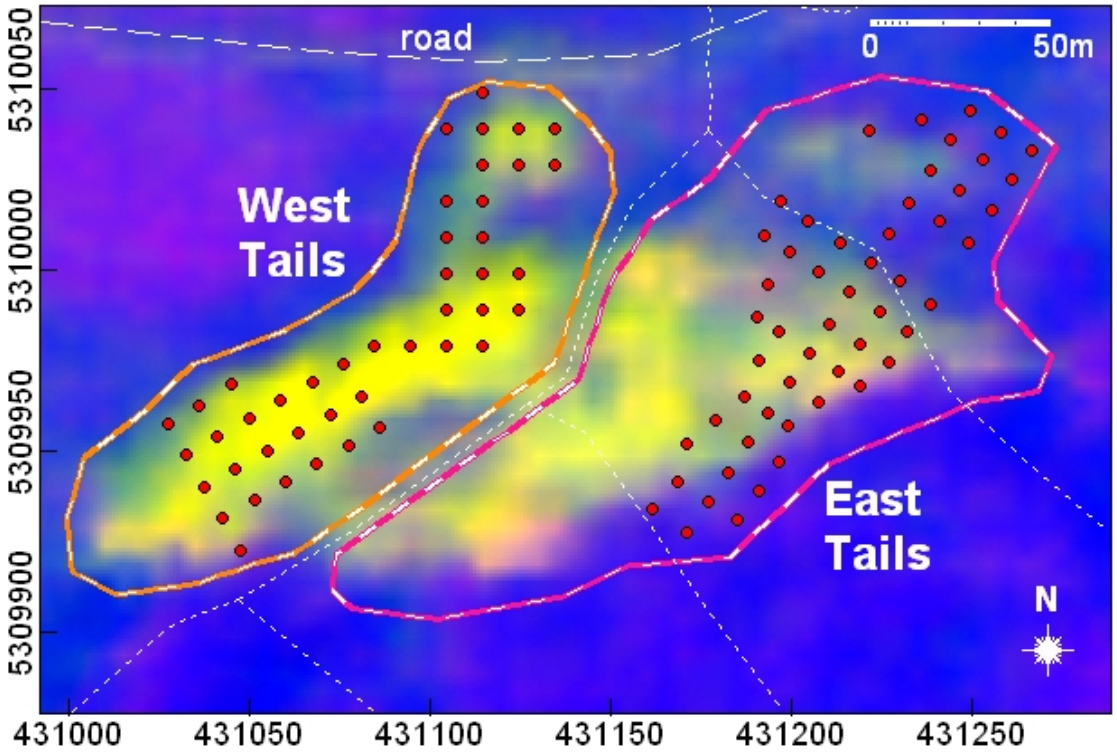

Figure: The "East Tails" and the "West Tails" shown in a color composite image of the DAIS data. Ratios of ch17 to ch28 (representing ferrihydrite reflectance and absorption peaks) was used as red band, ch13 to ch25 (representing jarosite reflectance and absorption peaks) was used as green band and ch32 to ch1 (representing non-iron-bearing minerals) was used as blue band. Red dots are locations of mine tailings samples. Short dashed lines indicates drainage lines of either active or non-active streams.

Table: Elementary statistics of original geochemical data and skewness of $\log_e$-transformed data — East tails. All concentrations are in ppm except where stated.

East Tails samples ($n = 53$):						
Element	Min	Max	Mean	SD	Skew	Skew ($\log_e$)
As	48.6	1568.0	266.3	273.9	2.74	0.67
Cd (ppb)	190.0	540.0	323.2	78.2	0.27	−0.28
Cu	85.5	1483.7	354.8	303.3	2.22	0.91
Fe (%)	1.5	3.7	2.8	0.4	-0.49	−1.11
Mn	17.7	766.4	128.4	140.2	3.17	0.41
Ni (ppb)	100.0	4340.0	1129.2	903.5	2.16	−0.36
Pb	14.0	251.8	50.9	52.1	2.27	0.92
Sb (ppb)	5.0	160.0	36.9	31.2	1.59	−0.17
Zn	42.6	762.8	124.4	111.8	3.96	1.14

Table: Elementary statistics of original geochemical data and skewness of $\log_e$-transformed data — West tails. All concentrations are in ppm except where stated.

West Tails samples ($n = 44$):						
Element	Min	Max	Mean	SD	Skew	Skew ($\log_e$)
As	196.3	2789.3	625.9	452.0	3.05	0.73
Cd (ppb)	140.0	720.0	275.7	121.8	2.42	1.19
Cu	303.0	2064.7	889.9	476.2	1.12	0.09
Fe (%)	1.4	3.2	2.3	0.4	0.40	−0.06
Mn	15.1	207.6	52.6	34.8	2.40	0.33
Ni (ppb)	60.0	1370.0	371.1	285.6	2.07	−0.06
Pb	40.4	806.9	192.0	169.8	2.24	0.47
Sb (ppb)	5.0	420.0	84.4	76.9	2.75	−0.31
Zn	68.7	776.7	275.2	179.6	1.18	0.06

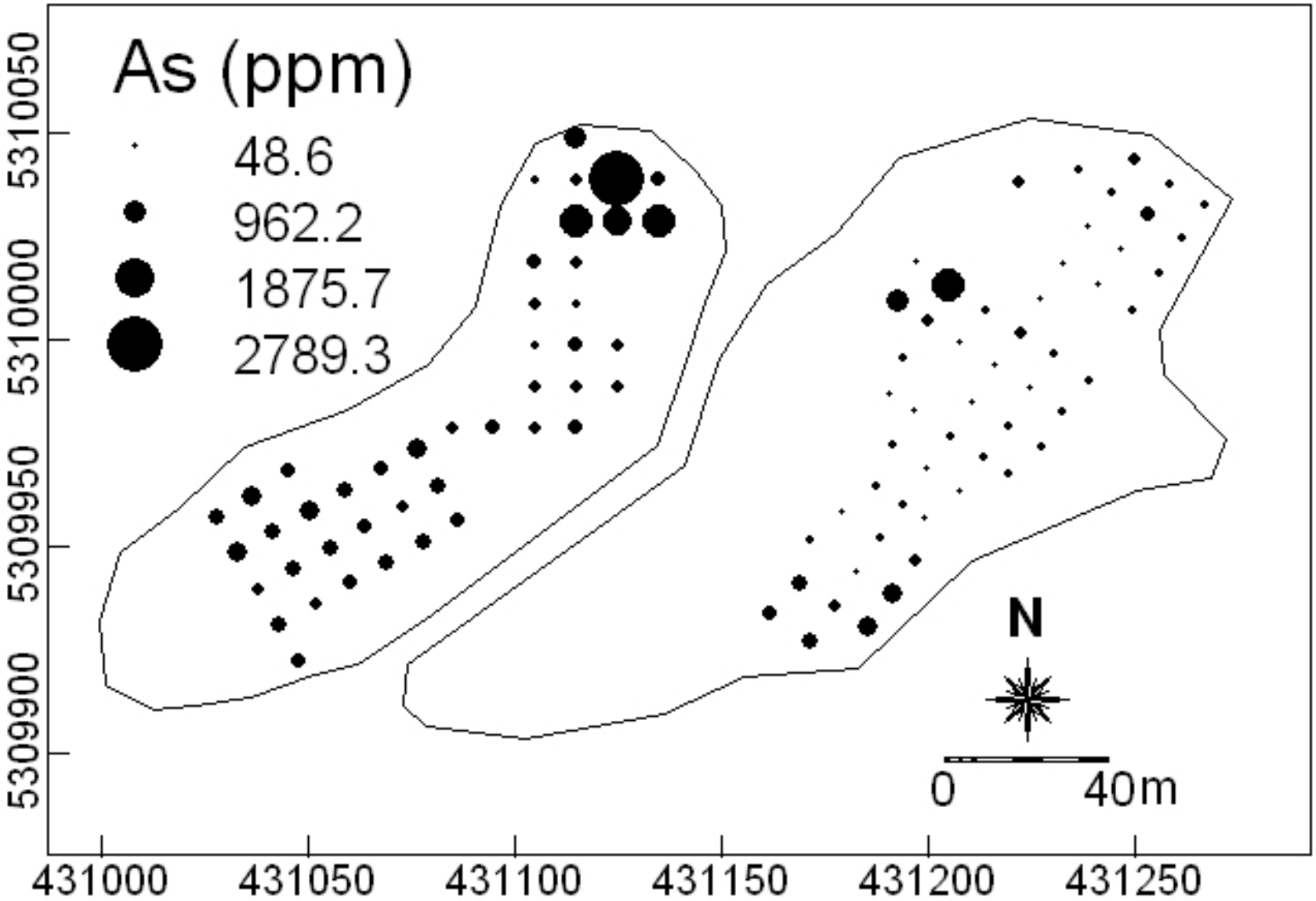
As (ppm)
48.6
962.2
1875.7
2789.3
N
0
40m
5310050
5310000
5309950
5309900
431000
431050
431100
431150
431200
431250

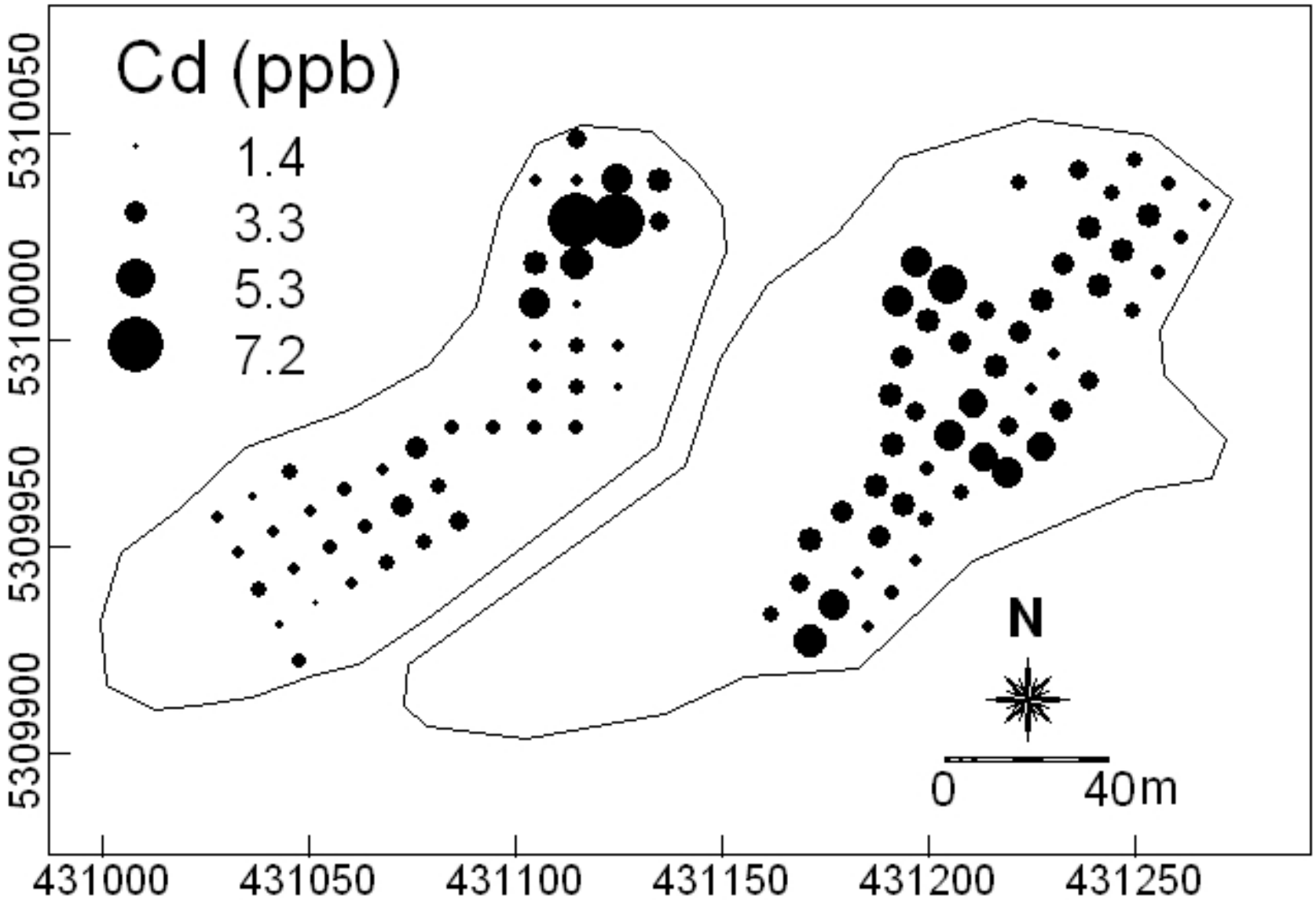
Cd (ppb)
1.4
3.3
5.3
7.2
N
0
40m
5310050
5310000
5309950
5309900
431000
431050
431100
431150
431200
431250

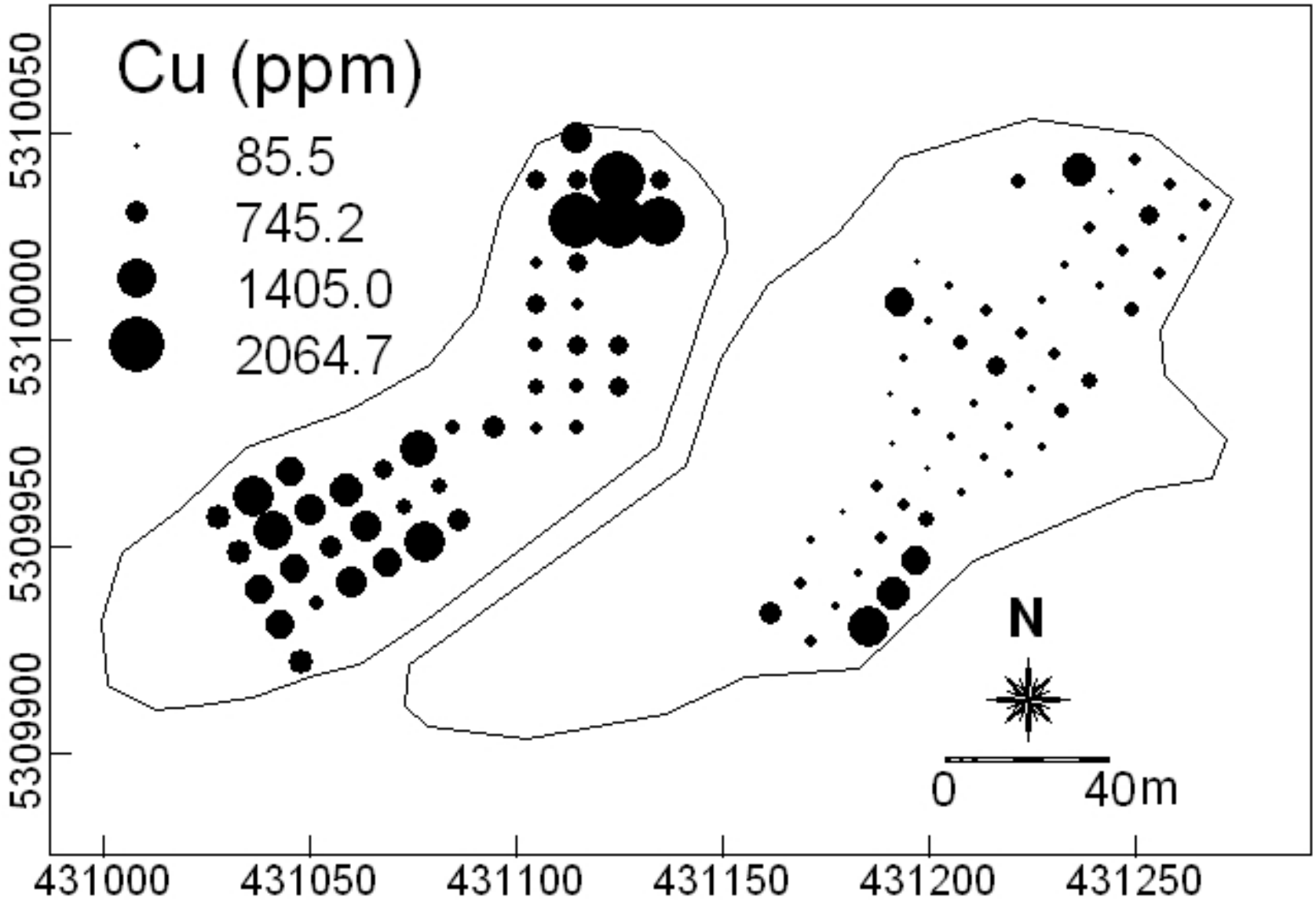
Cu (ppm)
85.5
745.2
1405.0
2064.7
N
0
40m
5310050
5310000
5309950
5309900
431000
431050
431100
431150
431200
431250

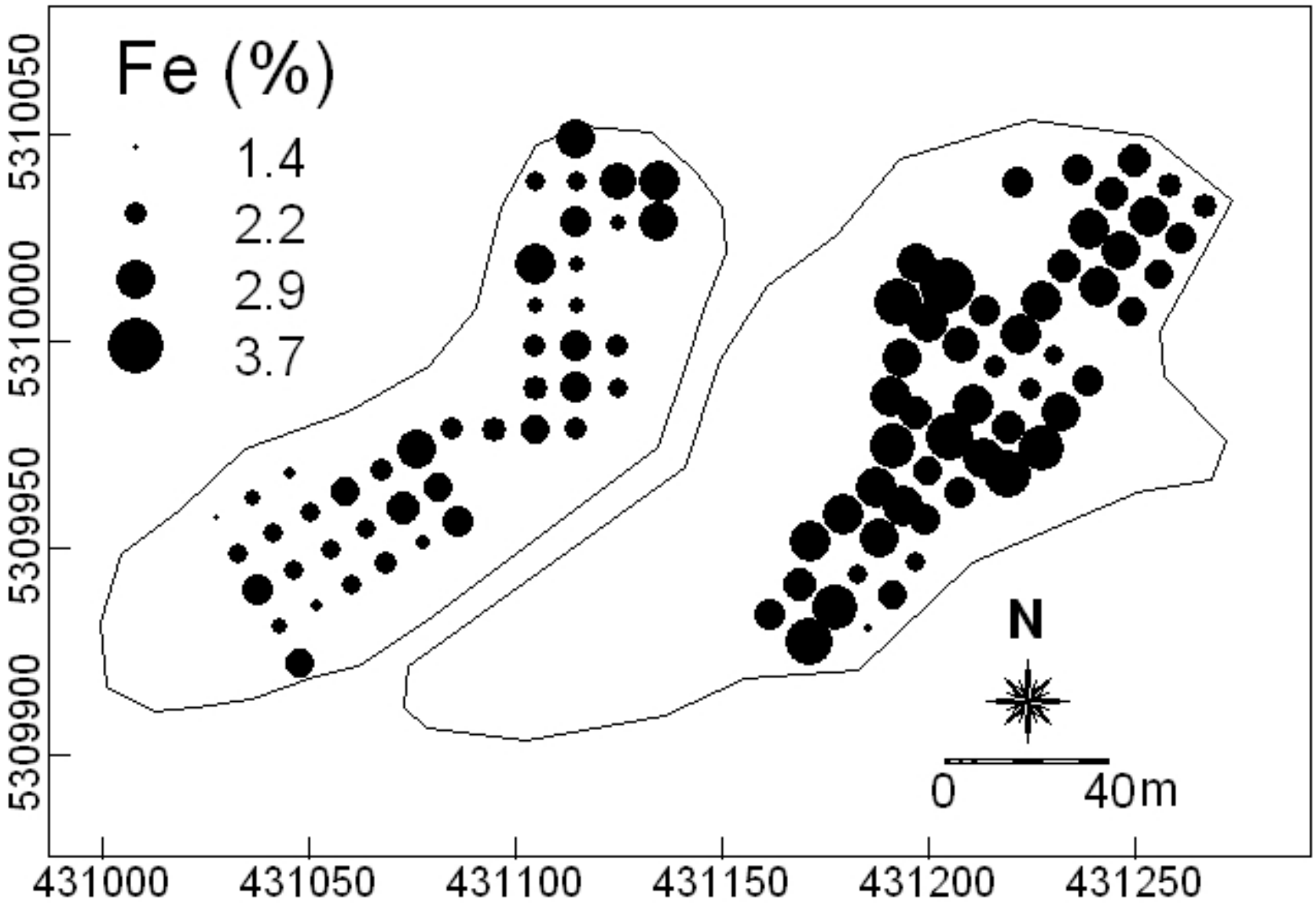
Fe (%)
1.4
2.2
2.9
3.7
N
0
40m
5310050
5310000
5309950
5309900
431000
431050
431100
431150
431200
431250

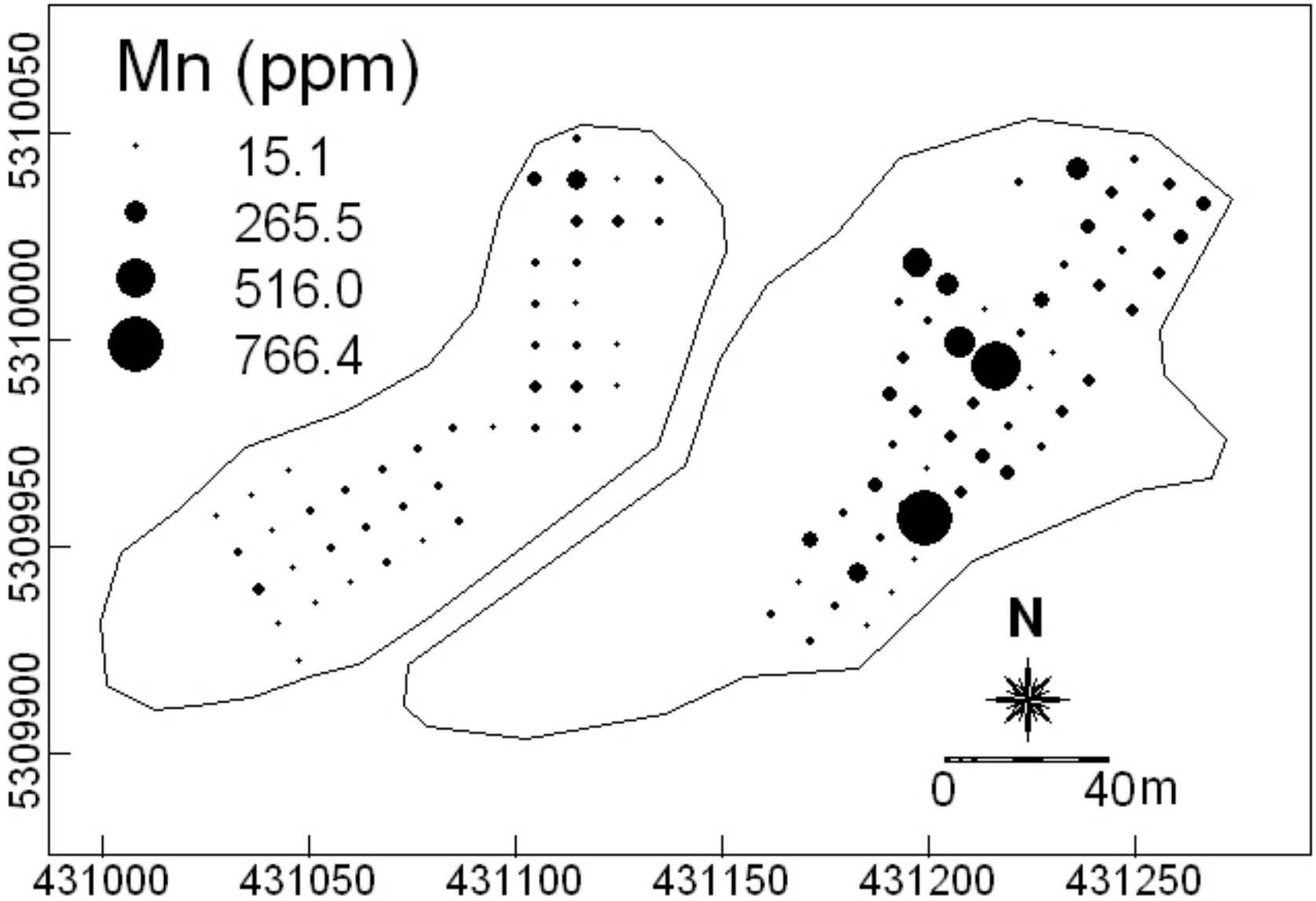
Mn (ppm)
15.1
265.5
516.0
766.4
N
0
40m
5310050
5310000
5309950
5309900
431000
431050
431100
431150
431200
431250

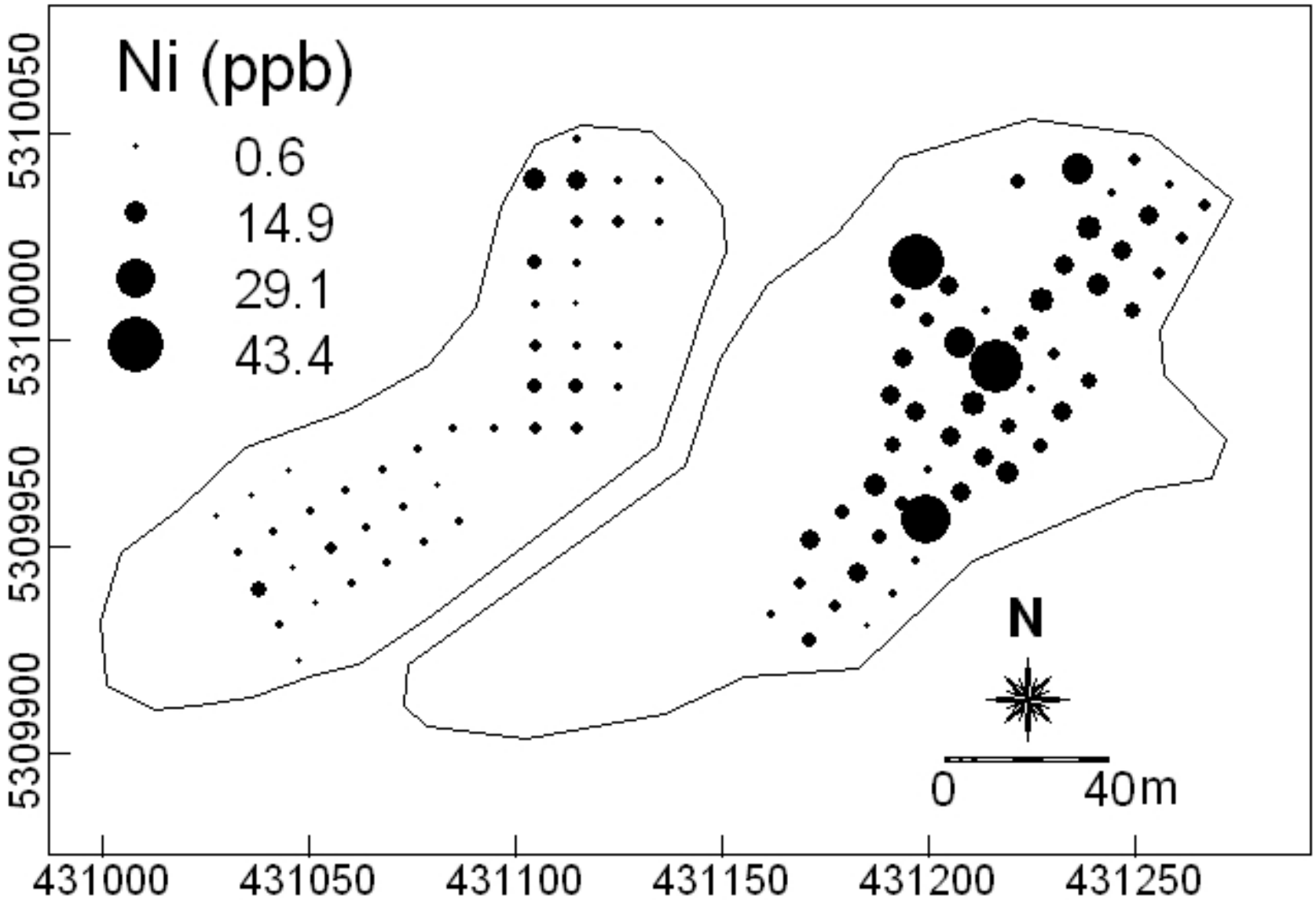
Ni (ppb)
0.6
14.9
29.1
43.4
N
0
40m
5310050
5310000
5309950
5309900
431000
431050
431100
431150
431200
431250

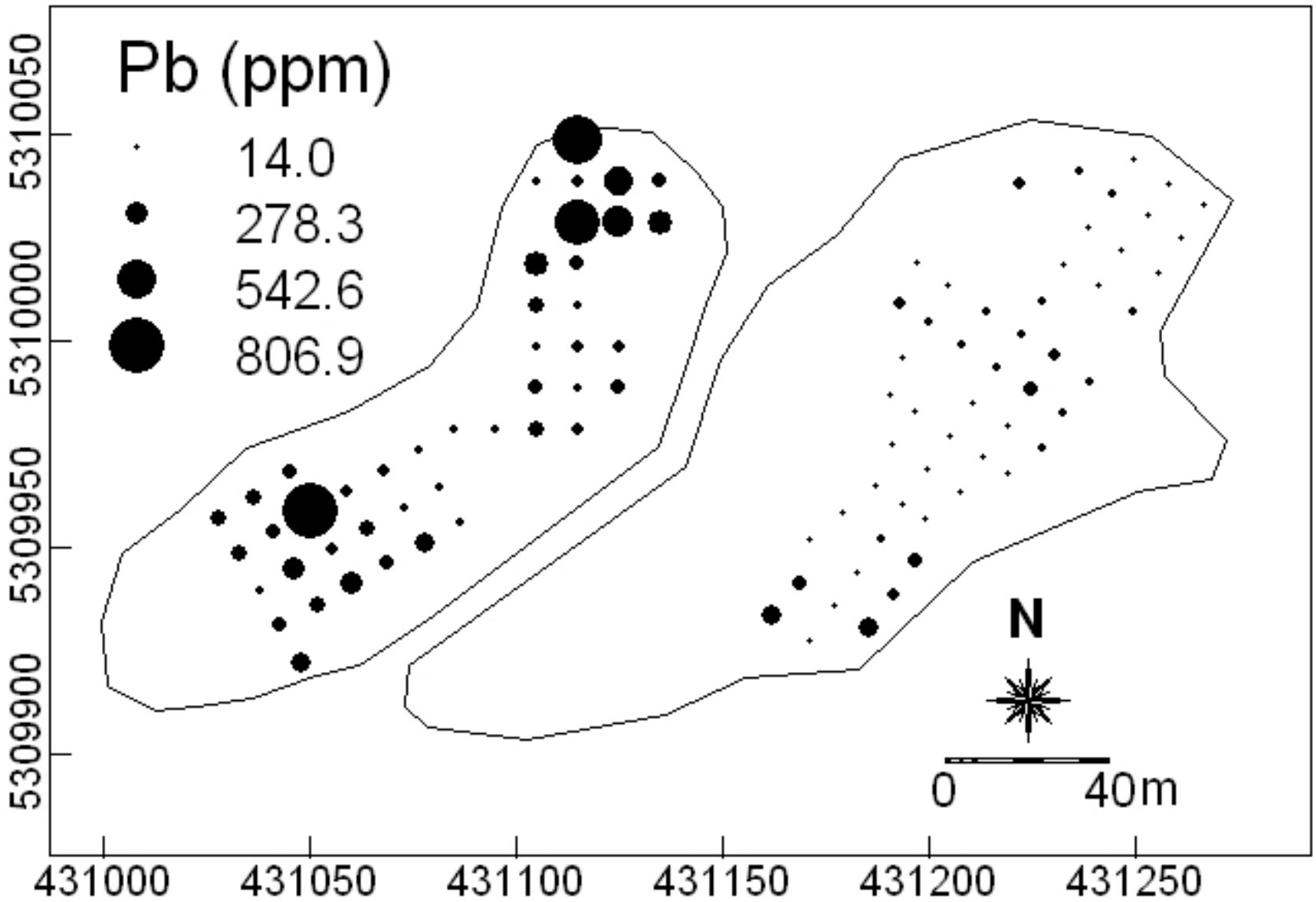
Pb (ppm)
14.0
278.3
542.6
806.9
N
0
40m
5310050
5310000
5309950
5309900
431000
431050
431100
431150
431200
431250

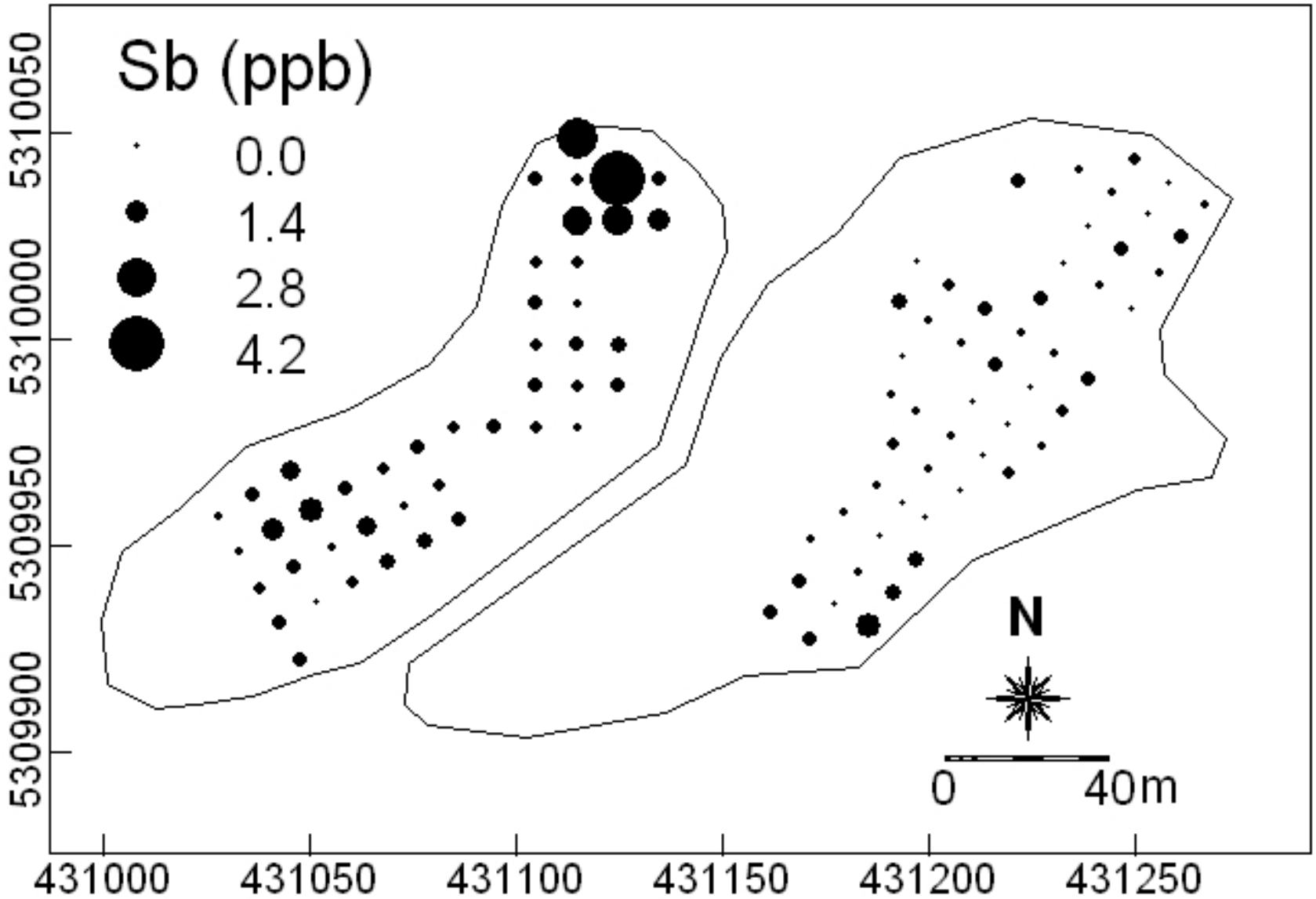
Sb (ppb)
0.0
1.4
2.8
4.2
N
0
40m
5310050
5310000
5309950
5309900
431000
431050
431100
431150
431200
431250

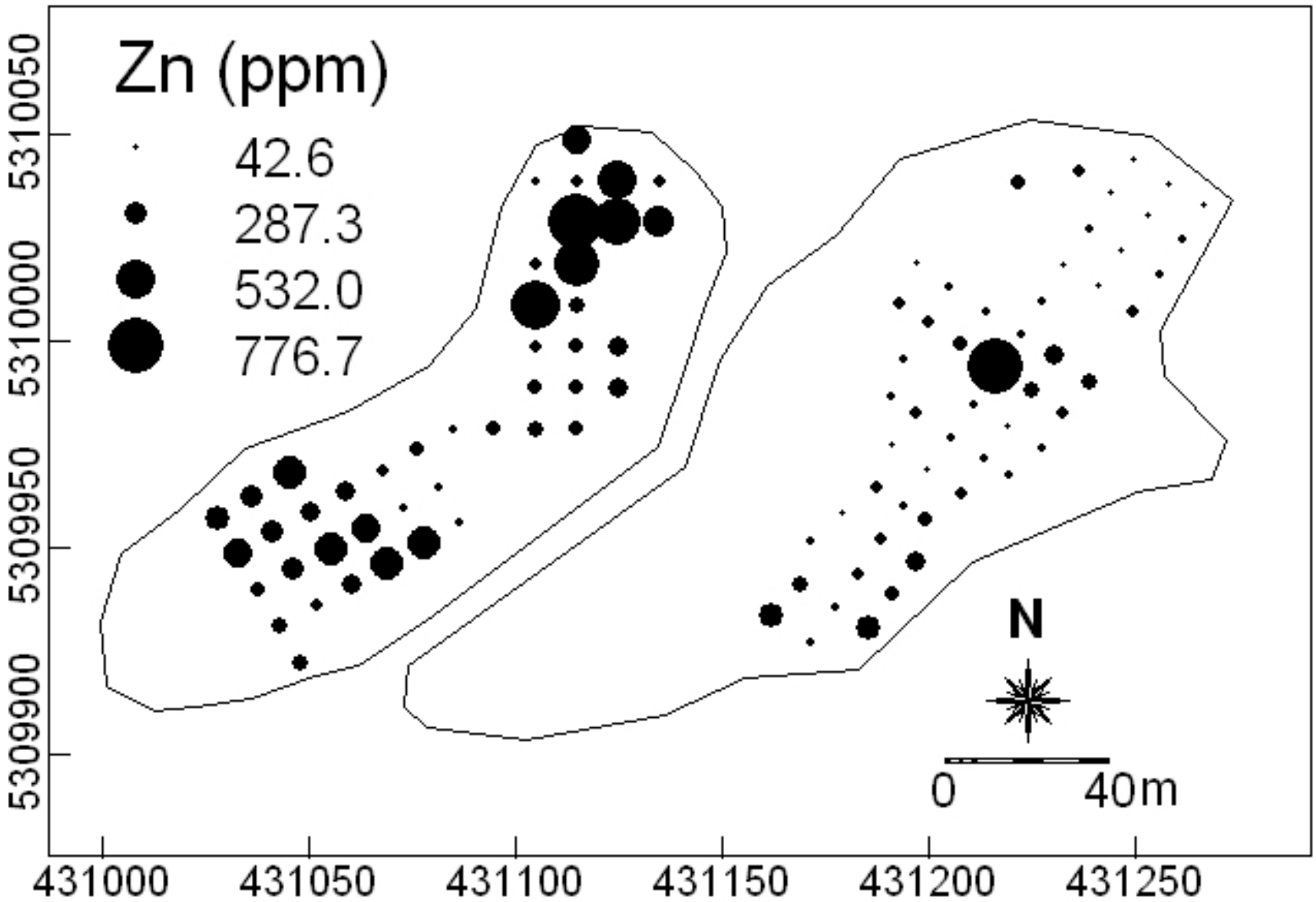
Zn (ppm)
42.6
287.3
532.0
776.7
N
0
40m
5310050
5310000
5309950
5309900
431000
431050
431100
431150
431200
431250

Splitting the Data

- The East and West Tails have different geochemical characteristics — split the data into two sets.
- Data from either sub-area are used to model a relationship between heavy metal associations and relative abundances of secondary iron-bearing minerals.
- The latter data are derived from spectral unmixing of hyperspectral data. See: Debba *et. al.* (2006). Abundance estimation of spectrally similar materials by using derivatives in simulated annealing, *IEEE Geoscience and Remote Sensing*, vol. 44, no. 12, 3649–3658.
- Endmembers considered copiapite, jarosite, goethite, ferrihydrite, hematite, kaolinite, anhydrite, gypsum, quartz, and tumbleweed (grass).

- A model relationship between heavy metal associations and mineral abundances in one sub-area is then used as basis for optimal sampling design in the same sub-area and in the other sub-area.
- Division of the area and the data thus provides calibration analysis and prediction/validation analysis for optimal sampling design.

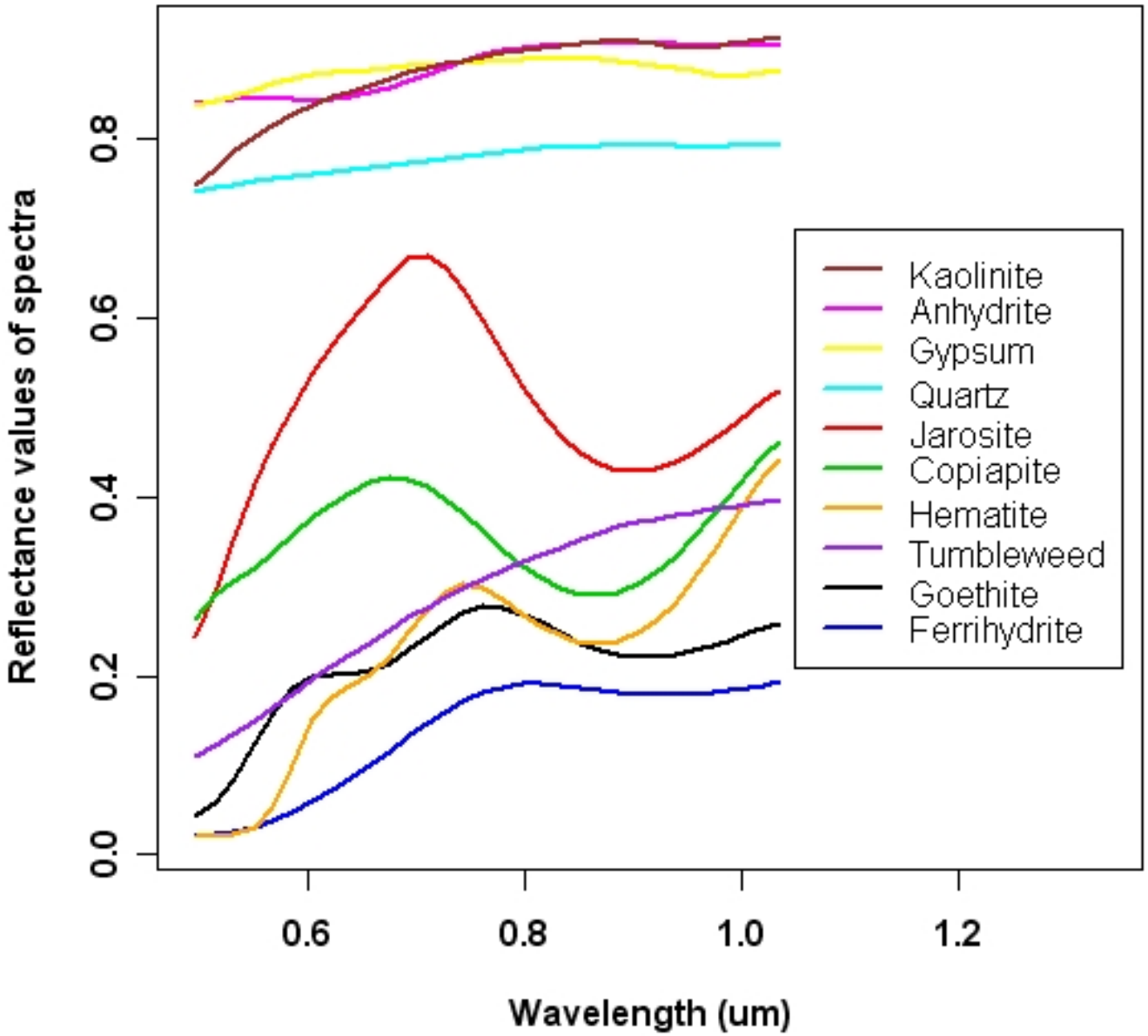

Figure: Reflectances of minerals which are common in contaminated areas.

Table: Elementary statistics of relative abundance estimates for end-members.

	East Tails Samples ($n = 53$)				West Tails Samples ($n = 44$)			
Endmember	Min	Max	Mean	SD	Min	Max	Mean	SD
goethite	0.00	0.21	0.04	0.05	0.00	0.18	0.04	0.05
jarosite	0.00	0.29	0.05	0.07	0.00	0.30	0.05	0.07
hematite	0.00	0.21	0.04	0.05	0.00	0.36	0.07	0.08
ferrihydrite	0.00	0.12	0.03	0.03	0.00	0.49	0.07	0.10
kaolinite	0.00	0.21	0.04	0.04	0.00	0.30	0.06	0.07
quartz	0.00	0.13	0.03	0.03	0.00	0.39	0.08	0.10
copiapite	0.00	0.16	0.04	0.04	0.00	0.33	0.06	0.07
gypsum	0.00	0.33	0.03	0.05	0.00	0.33	0.07	0.09
anhydrite	0.00	0.16	0.03	0.04	0.00	0.25	0.06	0.07
tumbelweed	0.00	0.18	0.03	0.04	0.00	0.45	0.07	0.08

Table: Elementary statistics of relative abundance estimates for end-members.

	East Tails HS ($n = 575$)				West Tails HS ($n = 383$)			
Endmember	Min	Max	Mean	SD	Min	Max	Mean	SD
goethite	0.00	0.36	0.04	0.05	0.00	0.42	0.05	0.05
jarosite	0.00	0.31	0.05	0.06	0.00	0.45	0.05	0.06
hematite	0.00	0.32	0.04	0.05	0.00	0.36	0.04	0.05
ferrihydrite	0.00	0.44	0.05	0.06	0.00	0.49	0.05	0.06
kaolinite	0.00	0.53	0.05	0.06	0.00	0.34	0.04	0.05
quartz	0.00	0.31	0.04	0.05	0.00	0.39	0.05	0.05
copiapite	0.00	0.32	0.05	0.06	0.00	0.36	0.04	0.06
gypsum	0.00	0.36	0.05	0.06	0.00	0.33	0.04	0.05
anhydrite	0.00	0.40	0.04	0.05	0.00	0.45	0.04	0.06
tumbelweed	0.00	0.37	0.04	0.05	0.00	0.45	0.05	0.06

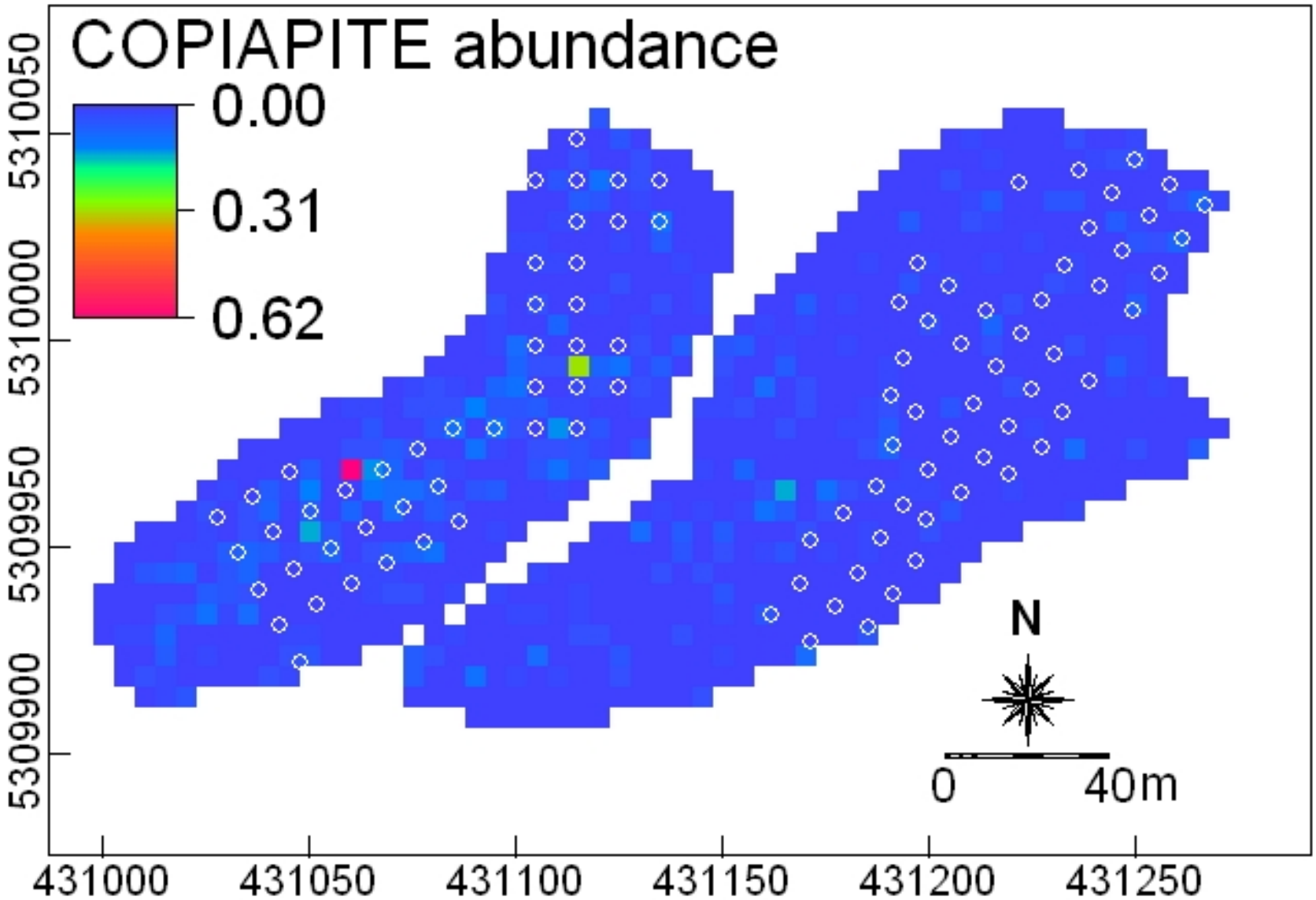
COPIAPITE abundance
0.00
0.31
0.62
5310050
5310000
5309950
5309900
431000
431050
431100
431150
431200
431250
N
0
40m

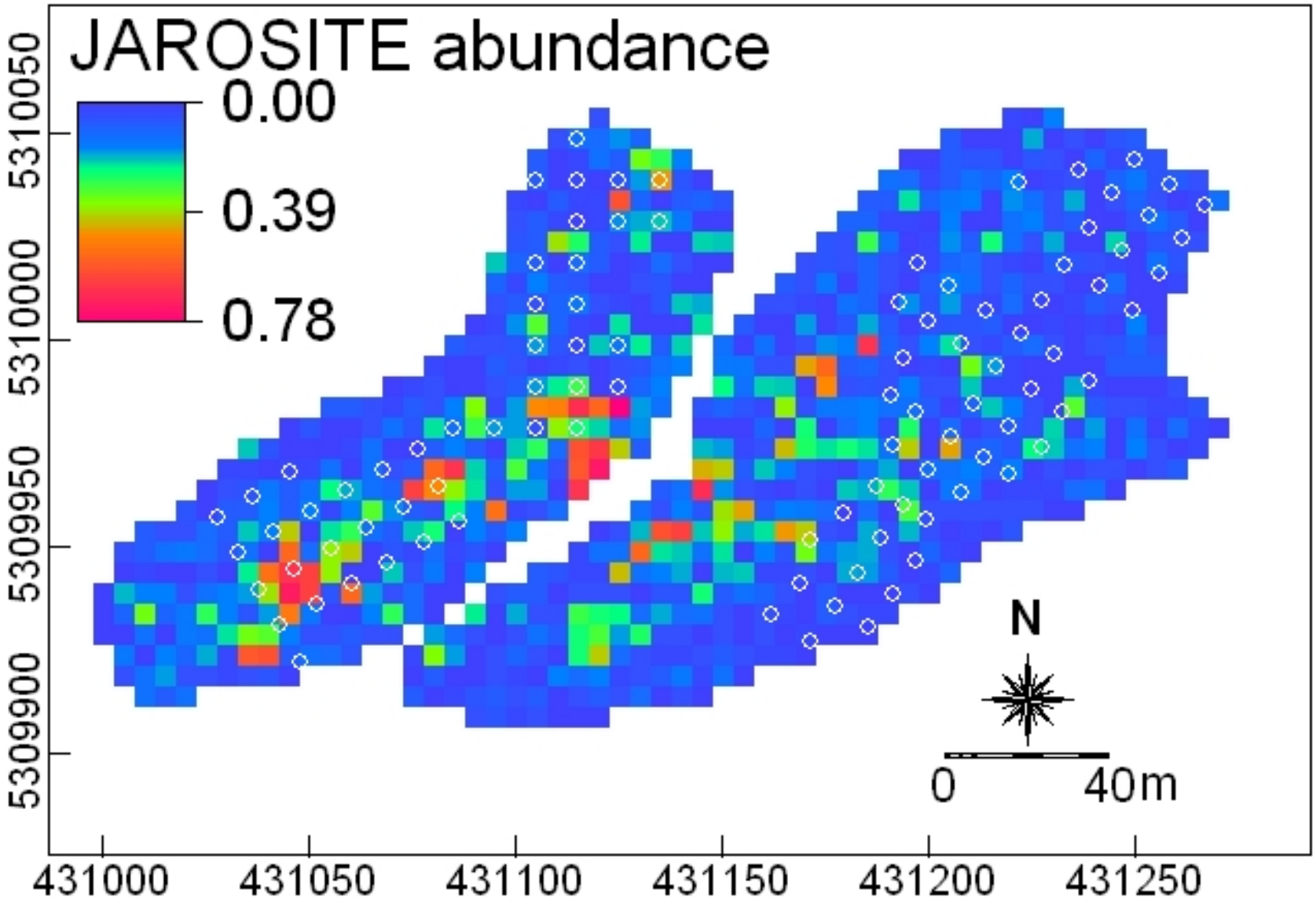
JAROSITE abundance
0.00
0.39
0.78
5310050
5310000
5309950
5309900
431000
431050
431100
431150
431200
431250
N
0
40m

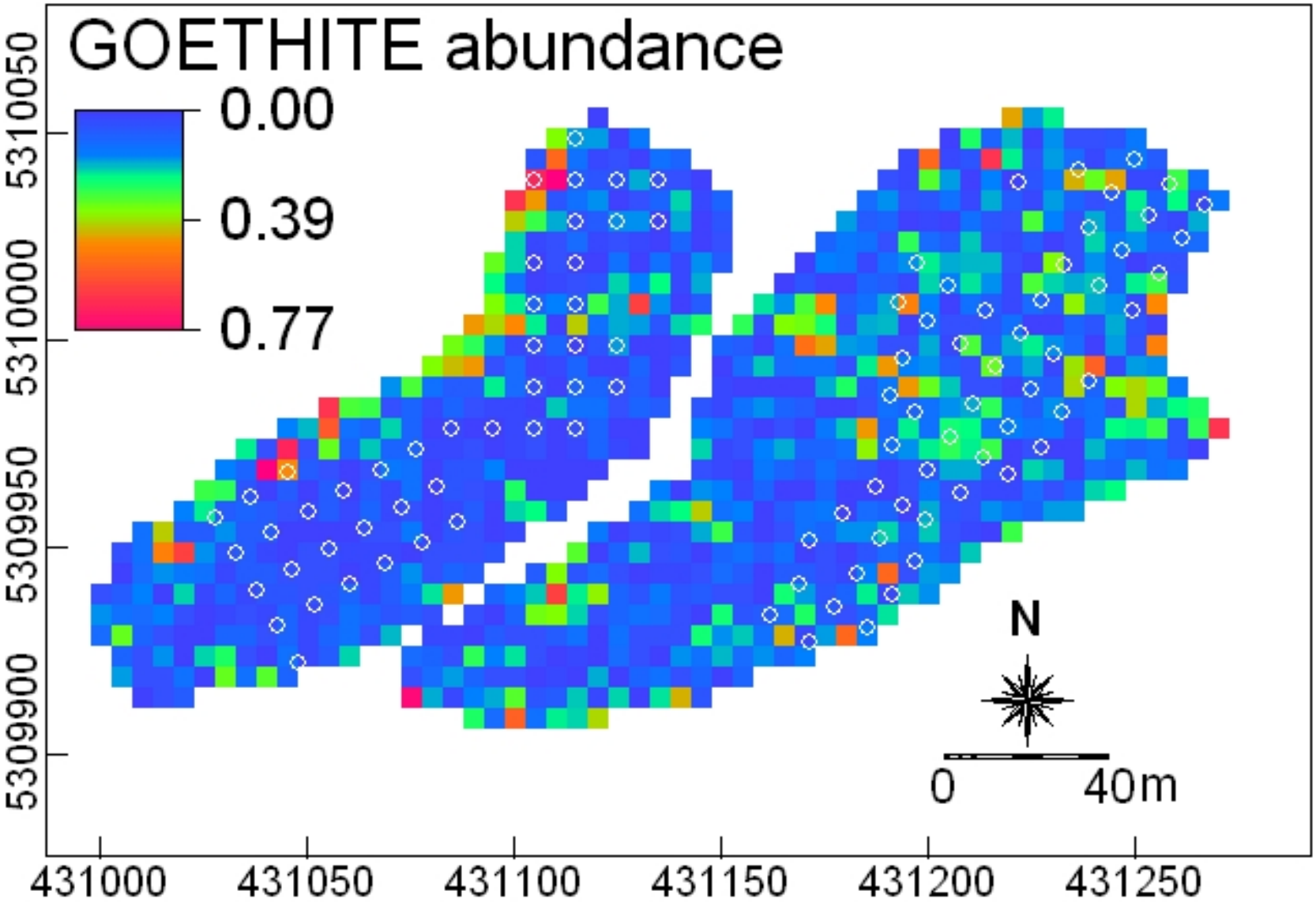
GOETHITE abundance
0.00
0.39
0.77
N
0
40m
5310050
5310000
5309950
5309900
431000
431050
431100
431150
431200
431250

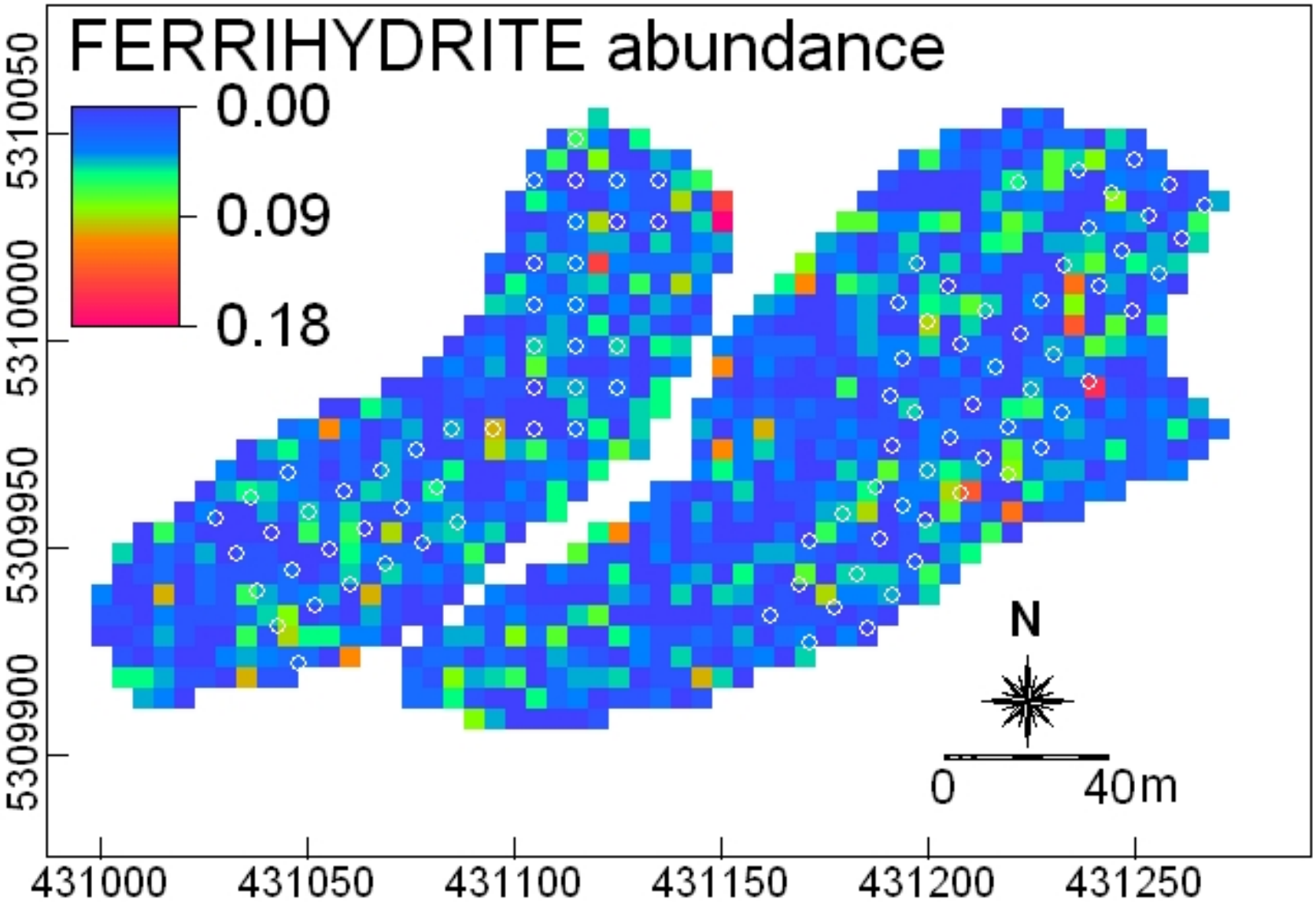
FERRIHYDRITE abundance
0.00
0.09
0.18
N
0
40m
5310050
5310000
5309950
5309900
431000
431050
431100
431150
431200
431250

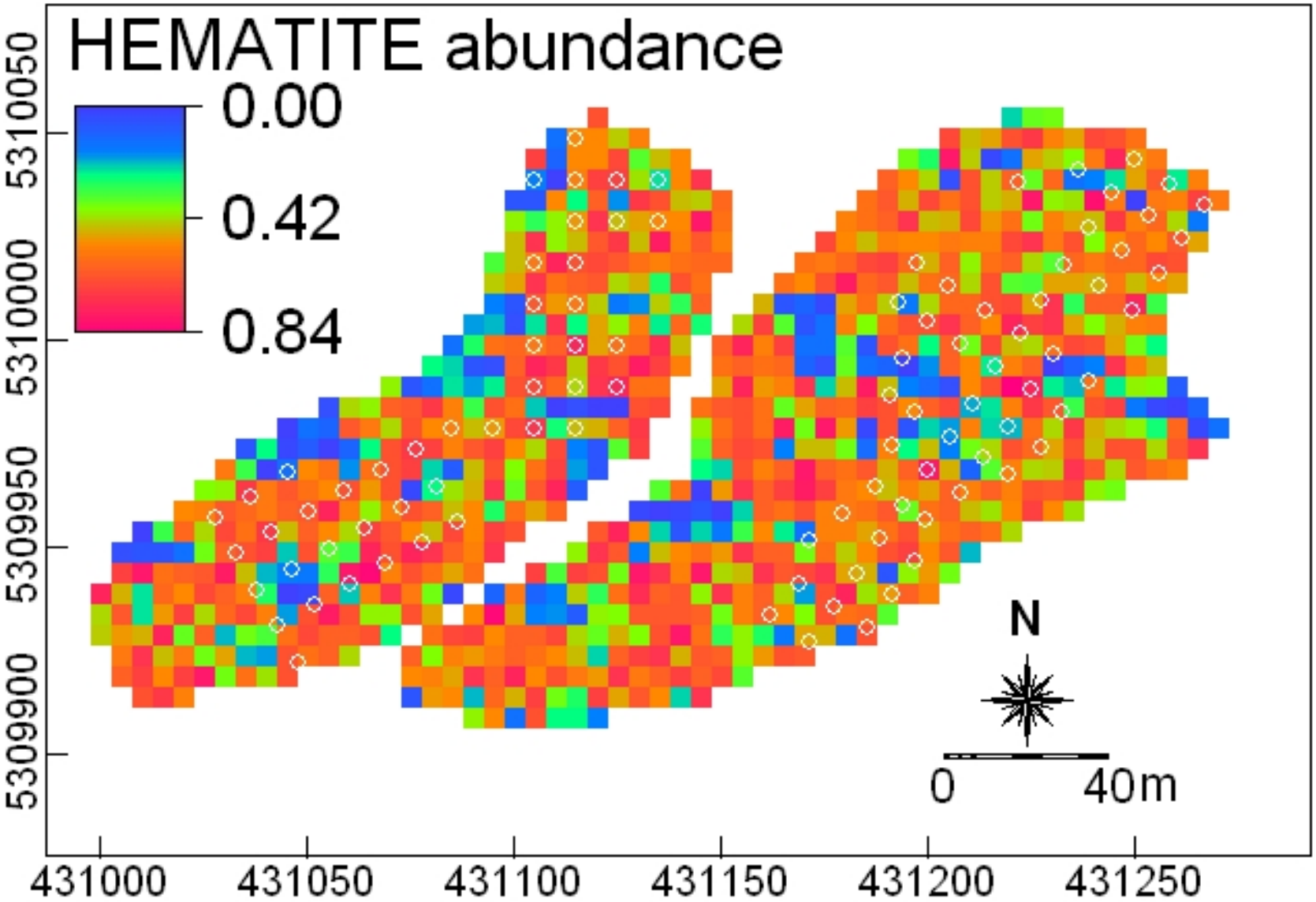
HEMATITE abundance
0.00
0.42
0.84
N
0
40m
5310050
5310000
5309950
5309900
431000
431050
431100
431150
431200
431250

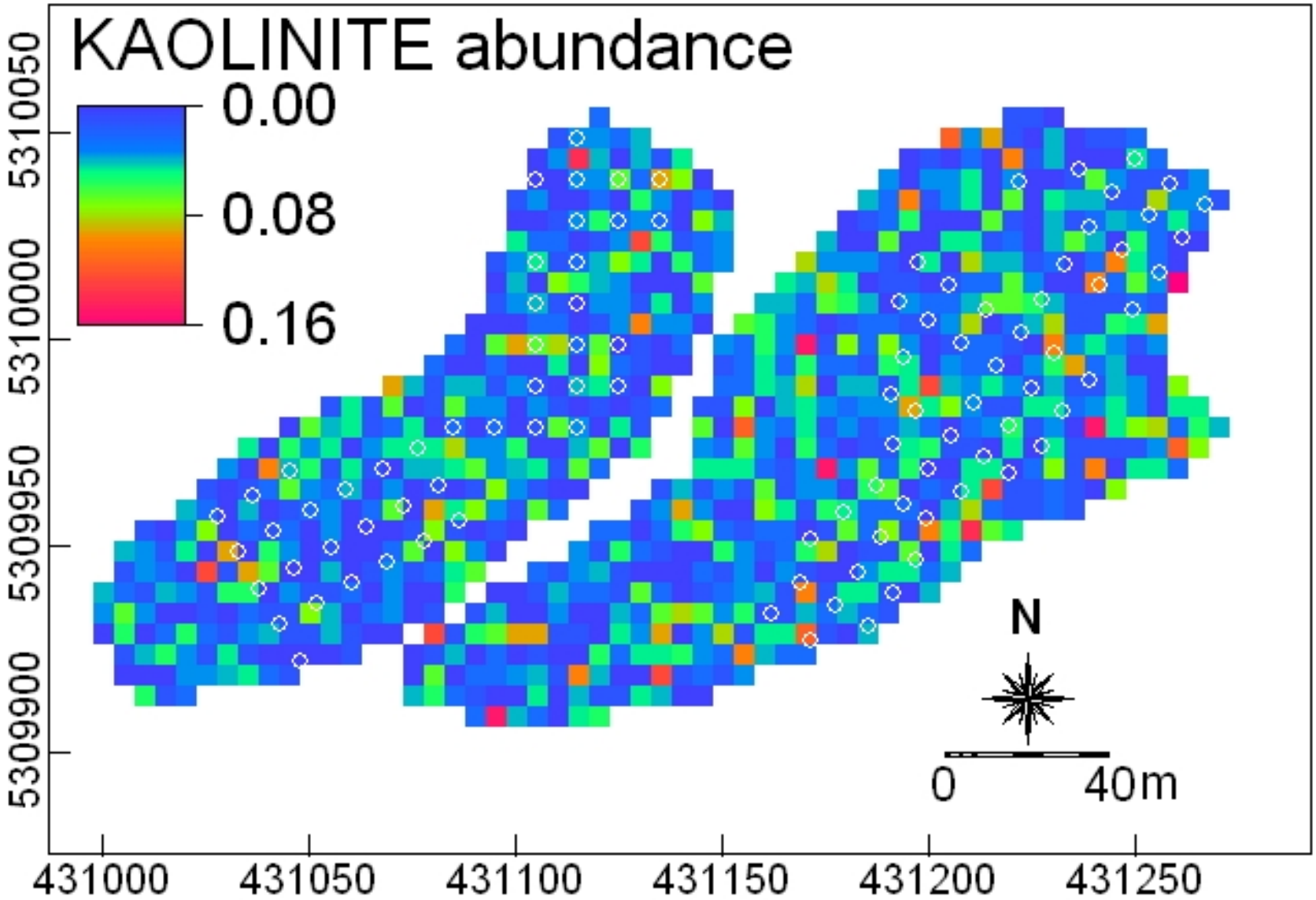
KAOLINITE abundance
0.00
0.08
0.16
N
0
40m
5310050
5310000
5309950
5309900
431000
431050
431100
431150
431200
431250

Modeling of heavy metal associations

- Concentrations of several metals in soils can be estimated using reflectance spectroscopy.
- Model heavy metals association reflecting scavenging of metals by secondary iron-bearing minerals in the mine tailings dumps.
- A factor component analysis with varimax rotation was performed on the logarithmic-transformed heavy metal concentrations to obtain the heavy metal association of interest.

Table: Factor component analysis with varimax rotation of the heavy metal concentrations.

East Tails ($n = 53$)										
Factor	As	Cd	Cu	Fe	Mn	Ni	Pb	Sb	Zn	var[a]
FA1	0.59	-0.13	0.82	-0.26	-0.02	-0.18	0.72	0.65	0.76	2.65
FA2	0.43	0.91	-0.23	0.91	0.15	0.32	-0.36	0.04	-0.43	2.34
FA3	-0.57	0.31	-0.3	0.13	0.92	0.90	-0.41	-0.17	0.14	2.33
West Tails ($n = 44$)										
Factor	As	Cd	Cu	Fe	Mn	Ni	Pb	Sb	Zn	var
FA1	0.90	0.56	0.86	0.10	-0.08	-0.27	0.76	0.71	0.79	3.65
FA2	0.01	0.58	-0.09	0.71	0.90	0.88	-0.07	0.35	-0.15	2.58

[a] Variance explained by each factor.

- FA1 of heavy metal contents in either the East Tails or the West Tails — show high positive loadings mostly on As, Cu, Pb, Sb, and Zn. This heavy metal association reflects the type of mineral deposits that were mined in the Recsk-Lahóca area. The As-Cu-Pb-Sb-Zn association therefore reflects the source materials of the mine tailings and/or the relatively unweathered parts of the mine tailings dumps.
- FA2 of heavy metal contents in either the East Tails or the West Tails shows high positive loadings on Fe. The FA2 also show that in either the East Tails or the West Tails there is a common heavy metal association of Fe-Cd-Ni-Mn. This heavy metal association reflects metal scavenging by not only secondary iron-bearing minerals but also secondary manganese bearing minerals.
- FA3 in the East Tails shows high positive loadings on Mn and Ni. This Mn-Ni association mainly reflects scavenging of Ni by secondary manganese oxides/hydroxides.

- The FA2 in both the East Tails and the West Tails are considered to represent the heavy metal association of interest. The second factor in the East Tails is labeled as FA2E and the second factor in the West Tails is labeled FA2W.
- Scores of FA2E AND FA2W were calculated using the corresponding factor component loadings.
- The scores of FA2E and FA2W — linearly transformed to $[0, 1]$ (for numerical compatibility with the mineral abundance estimates) — FA2ET and FA2WT.

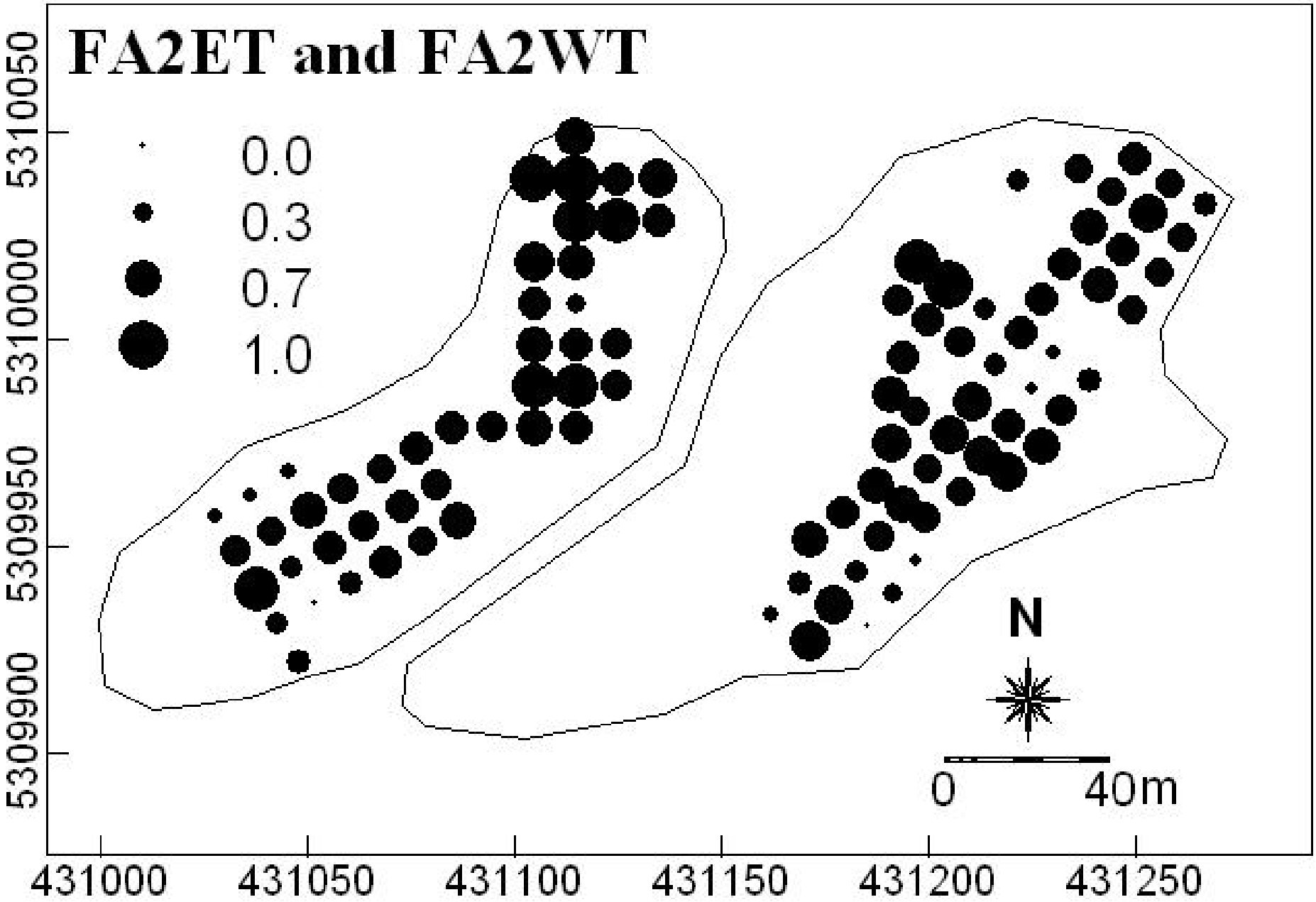
FA2ET and FA2WT
0.0
0.3
0.7
1.0
N
0
40m
5310050
5310000
5309950
5309900
431000
431050
431100
431150
431200
431250

Kriging with external drift

- Kriging with external drift is applicable to estimate primary variables of interest, which are practically measurable at only few sample sites, based on linearly related ancillary variables, which are measurable at much higher sampling density than the primary variables.
- Kriging with external drift is ideal if a primary variable could be measured more precisely and practically at a few locations (factor scores of heavy metal associations), whereas possibly less accurate measurements of linearly related ancillary variables are available everywhere in the spatial domain (relative abundances of metal-scavenging iron-bearing minerals – hyperspectral image).
- For the modeling, consider $\mathbf{x} \in \mathbf{A} \subset \mathbb{R}^2$ to be a generic data location (x_u, x_v) in 2-dimensional Euclidean space and suppose the domain $Z(\mathbf{x})$ at spatial location $\mathbf{x}$ is a random quantity.
- The multivariate random field $\{Z(\mathbf{x}) : \mathbf{x} \in \mathbf{A}\}$, is generated by letting $\mathbf{x}$ vary over index set $\mathbf{A} \subset \mathbb{R}^2$. A realization of this is denoted by $\{z(\mathbf{x}) : \mathbf{x} \in \mathbf{A}\}$.

Kriging with external drift

- The variogram
$$2\gamma(h) = E[Z(\mathbf{x}) - Z(\mathbf{x}+h)]^2 \ . \tag{1}$$
- The semi-variogram $\gamma(h)$:
$$\gamma(h) = \frac{1}{2}E[Z(\mathbf{x}) - Z(\mathbf{x}+h)]^2 \ . \tag{2}$$
- The experimental semi-variogram $\gamma^\star(h)$, where h is a fixed lag vector in both distance and direction, may be obtained from $\kappa = 1, 2, \ldots, P(h)$ pairs of observations $\{z(\mathbf{x}_\kappa), z(\mathbf{x}_\kappa + h)\}$ at locations $\{\mathbf{x}_\kappa, \mathbf{x}_\kappa + h\}$, as:
$$\gamma^\star(h) = \frac{1}{2 \cdot P(h)} \sum_{\kappa=1}^{P(h)} [z(\mathbf{x}_\kappa) - z(\mathbf{x}_\kappa + h)]^2 \ . \tag{3}$$

Kriging with external drift

- The k ancillary variables represented as regionalized variables $y_i(\mathbf{x}),\ i = 1, \ldots, k$ with n_A observations, are less accurate measurements covering the whole domain $\mathbf{A}$ at small scale and are considered as deterministic. The values $\{y_i(\mathbf{x})\}$ needs to be known at all locations $\mathbf{x}_\alpha$ of the samples as well as at the nodes of the estimation grid.
- Since $Z(\mathbf{x})$ and the set of $\{y_i(\mathbf{x})\}$ are two ways of expressing the same phenomenon, assume that $Z(\mathbf{x})$ is an average equal to a linear function of the set of $\{y_i(\mathbf{x})\}$ up to a constant b_0 and coefficients $b_i,\ i = 1, \ldots, k$,

$$E[Z(\mathbf{x})] = b_0 + \sum_{i=1}^{k} b_i \cdot y_i(\mathbf{x}) = \sum_{i=0}^{k} b_i \cdot y_i(\mathbf{x}) \ , \tag{4}$$

where $y_0(\mathbf{x}) = 1$.

Kriging with external drift

- Assuming $Z(\mathbf{x})$ is a second order stationary random function, then

$$Z^*(\mathbf{x}_0) = \sum_{\alpha=1}^{n_A} \lambda_\alpha Z(\mathbf{x}_\alpha) \tag{5}$$

where λ_α denotes the weight of the αth observation and is constraint to unit sum.

- In estimating the external drift coefficients, the following conditions,

$$\sum_{\alpha=1}^{n_A} \lambda_\alpha y_i(\mathbf{x}_\alpha) = y_i(\mathbf{x}_0) \ , \qquad i = 1, \ldots, k \ , \tag{6}$$

are added to the kriging system independently of the inference of the covariance function, hence the term "external".

- The kriging variance can then be written as

$$\sigma^2_{\mathrm{KED}}(\mathbf{x}_0) = \mathrm{Var}[Z(\mathbf{x}_0) - Z^*(\mathbf{x}_0)] \ . \tag{7}$$

Kriging with external drift

- The only factor influencing the kriging variance are the variogram $\gamma(h)$, the number of observations n_A, the sampling locations $\mathbf{x}_\alpha$ and the location $\mathbf{x}_0$. This means that the kriging variance does not depend on the observations themselves, but rather only on their relative spacing. The advantage is that in can be used to optimize sampling schemes in advance of data collection.
- The location and the covariates as external drift were used to estimate the heavy metal concentration,

$$\begin{aligned} E[Z(\mathbf{x})] &= b_0 + b_1 \cdot x_u + b_2 \cdot x_v + b_3 \cdot \mathrm{GOE}(\mathbf{x}) \\ &\quad + b_4 \cdot \mathrm{JAR}(\mathbf{x}) + b_5 \cdot \mathrm{FER}(\mathbf{x}) + b_6 \cdot \mathrm{HEM}(\mathbf{x}) \\ &\quad + b_7 \cdot \mathrm{KAO}(\mathbf{x}) + b_8 \cdot \mathrm{COP}(\mathbf{x}), \end{aligned} \tag{8}$$

namely, a first order polynomial on the coordinates and the abundance estimates of the metal-scavenging minerals.

Retrospective sampling: Sequential removal

- Mean Kriging Prediction Error (MKPE):

$$\phi_{\mathrm{MKPE}}(\mathbf{S}) = \frac{1}{n_p} \sum_{\mathbf{x} \in \mathbf{A}} \{Z(\mathbf{x}) - Z^*(\mathbf{x}|\mathbf{S})]\}^2 \ , \tag{9}$$

  where n_p is the number of observations in the sampling scheme, $Z(\mathbf{x})$ is the primary variable at location $\mathbf{x}$ and $Z^*(\mathbf{x}|\mathbf{S})$ is the predicted value at $\mathbf{x}$ for sampling scheme $\mathbf{S}$ with n_p samples.
- Removal of samples from an existing design to achieve an optimal retrospective sampling scheme.
- Samples discarded if its removal contributes to a highest increase in MKPE value.

Retrospective sampling: Simulated Annealing

- Mean Kriging Prediction Error (MKPE):

$$\phi_{\mathrm{MKPE}}(\mathbf{S}) = \frac{1}{n_p} \sum_{\mathbf{x} \in \mathbf{A}} \{Z(\mathbf{x}) - Z^*(\mathbf{x}|\mathbf{S})]\}^2 \ , \tag{10}$$

Prospective sampling: Simulated annealing

- The optimization procedure by simulated annealing is then performed by application of a criterion called the Mean Kriging Variance with External Drift (MKVED), the fitness function of which is defined as

$$\phi_{\mathrm{MKVED}}(\mathbf{S}) = \frac{1}{n_{\mathbf{A}}} \sum_{j=1}^{n_{\mathbf{A}}} \sigma^2_{\mathrm{KED}}(\mathbf{x}_{\mathbf{A},j}|\mathbf{S}) \ , \tag{11}$$

  where $n_{\mathbf{A}}$ is the number of raster nodes for which data for each of the covariates are available.
- The MKVED-criterion is proposed to derive the optimal prospective sampling scheme in an unvisited area based on a relevant model from a previously sampled area.

Retrospective sampling: Sequential removal

- Ten sequential removals were made to derive an optimal retrospective sampling scheme with 43 samples for the East Tails and an optimal retrospective sampling scheme with 34 samples for the West Tails.
- For the East Tails, remaining 43 samples gave a mean prediction error of 6.34×10^{-7}.
- For the West Tails, remaining 34 samples gave a mean prediction error of 1.36×10^{-6}.

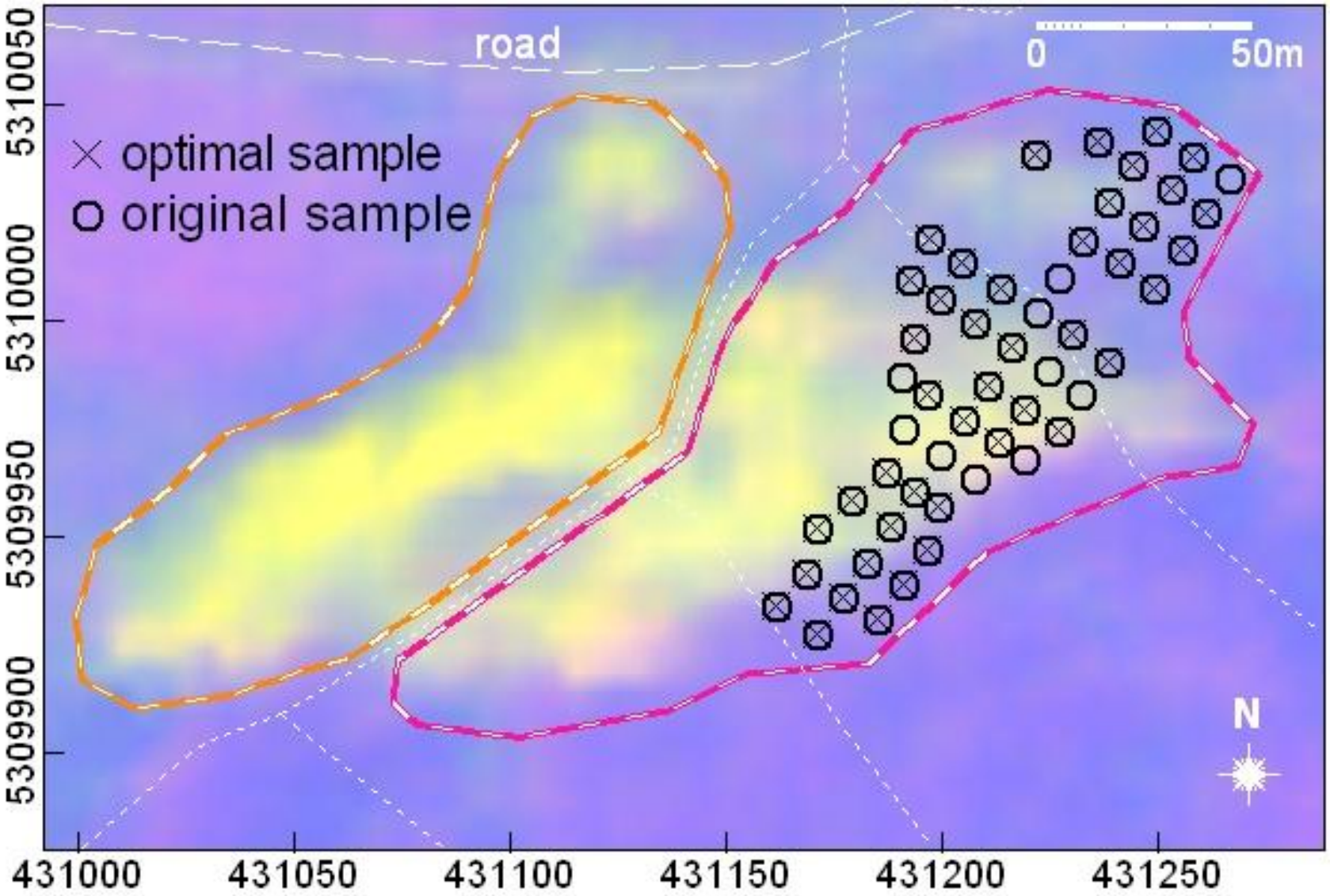

Figure: Sequential removal — East tails

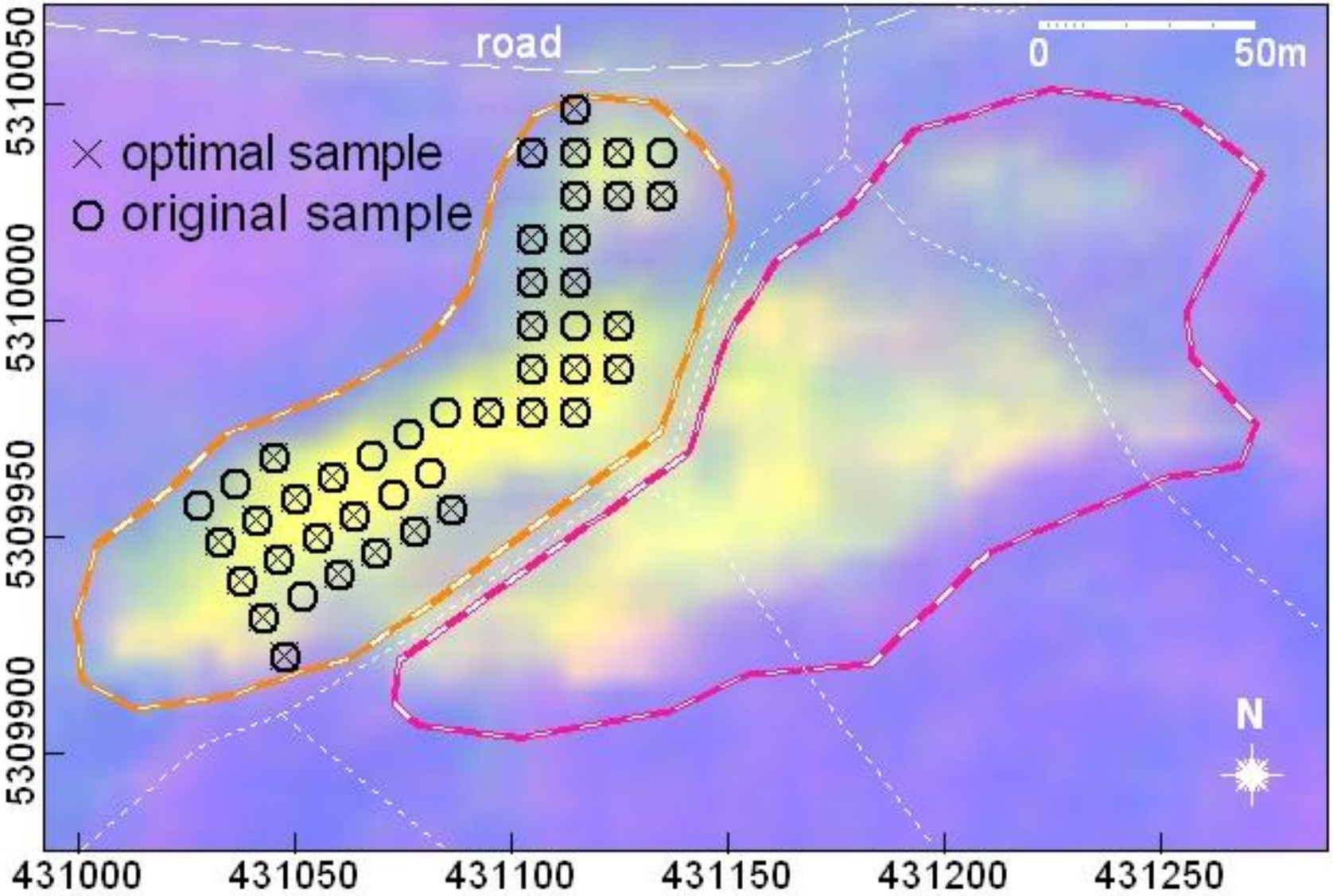

Figure: Sequential removal — West tails

Retrospective sampling: Simulated Annealing

- Sampling scheme with 10 samples less than an existing sampling scheme.
- For the East Tails, remaining 43 samples gave a mean prediction error of 2.75×10^{-16}.
- For the West Tails, remaining 34 samples gave a mean prediction error of 1.17×10^{-14}.
- Clearly, optimized retrospective sampling schemes derived via simulated annealing have considerably lower prediction errors than optimized retrospective samples schemes derived by sequential removal of samples.

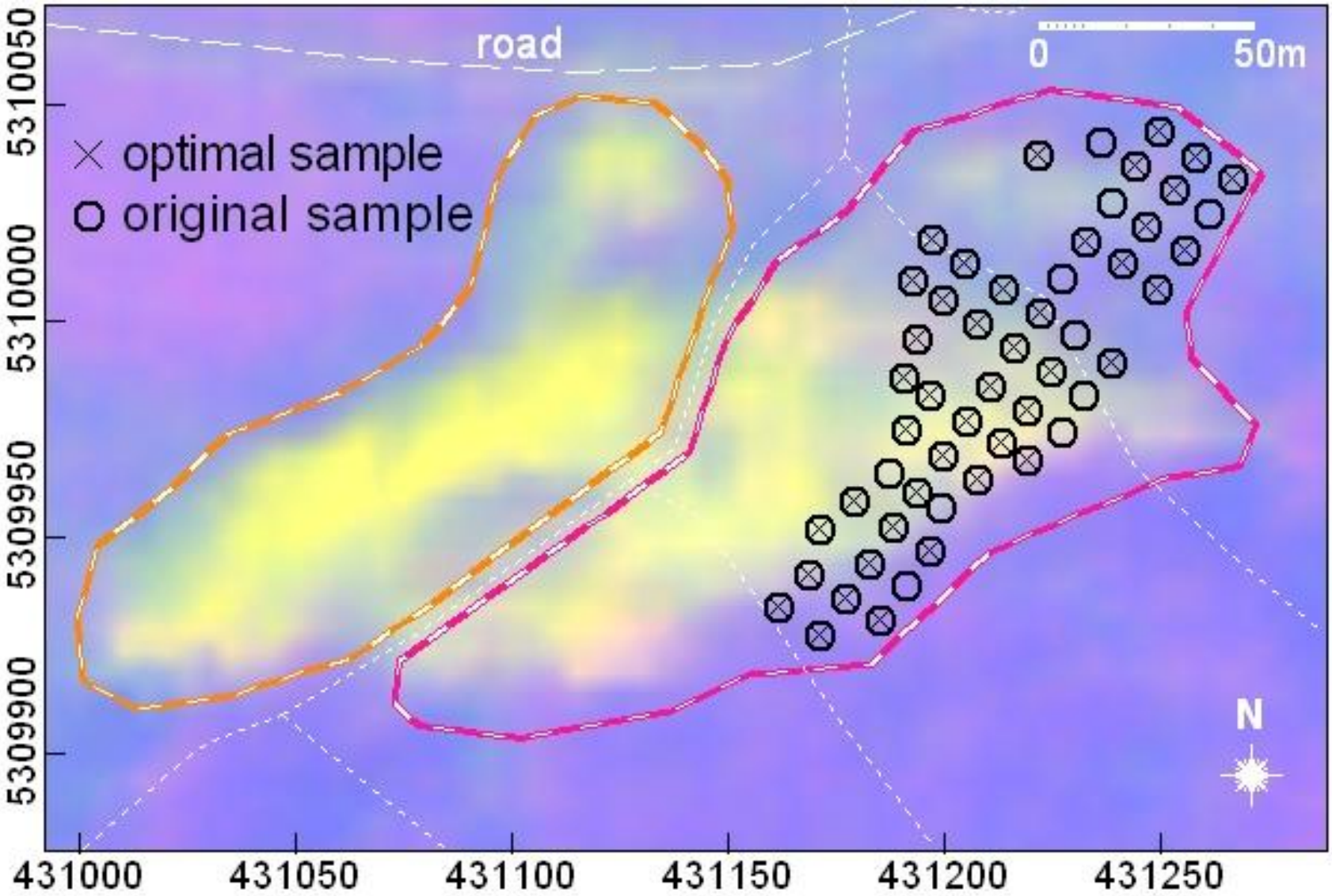

Figure: Simulated Annealing — East tails

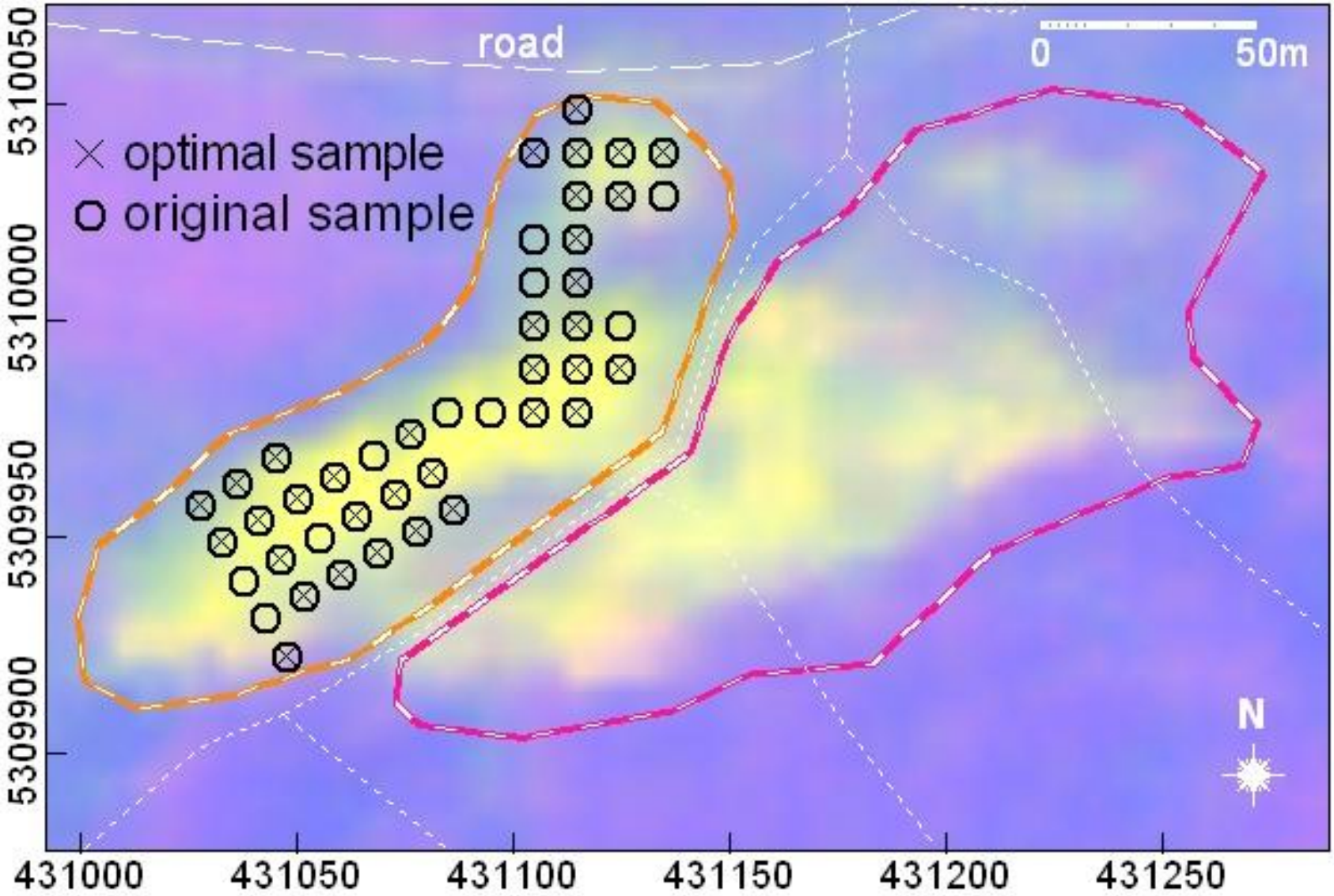

Figure: Simulated Annealing — West tails

A prospective sampling scheme

- A prospective sampling scheme for the West Tails is derived based on a model for the East Tails.
- As an illustration, it was decided to derive a prospective sampling scheme having 30 samples in the West Tails using the 53 samples from the East Tails.
- The exponential variogram was estimated with the data from the East Tails.
- To verify that this variogram is also appropriate for the West Tails, the East and West Tails data were combined.
- The similarity of the two variograms indicate that the variogram for the East Tails could be appropriate for modeling the West Tails.

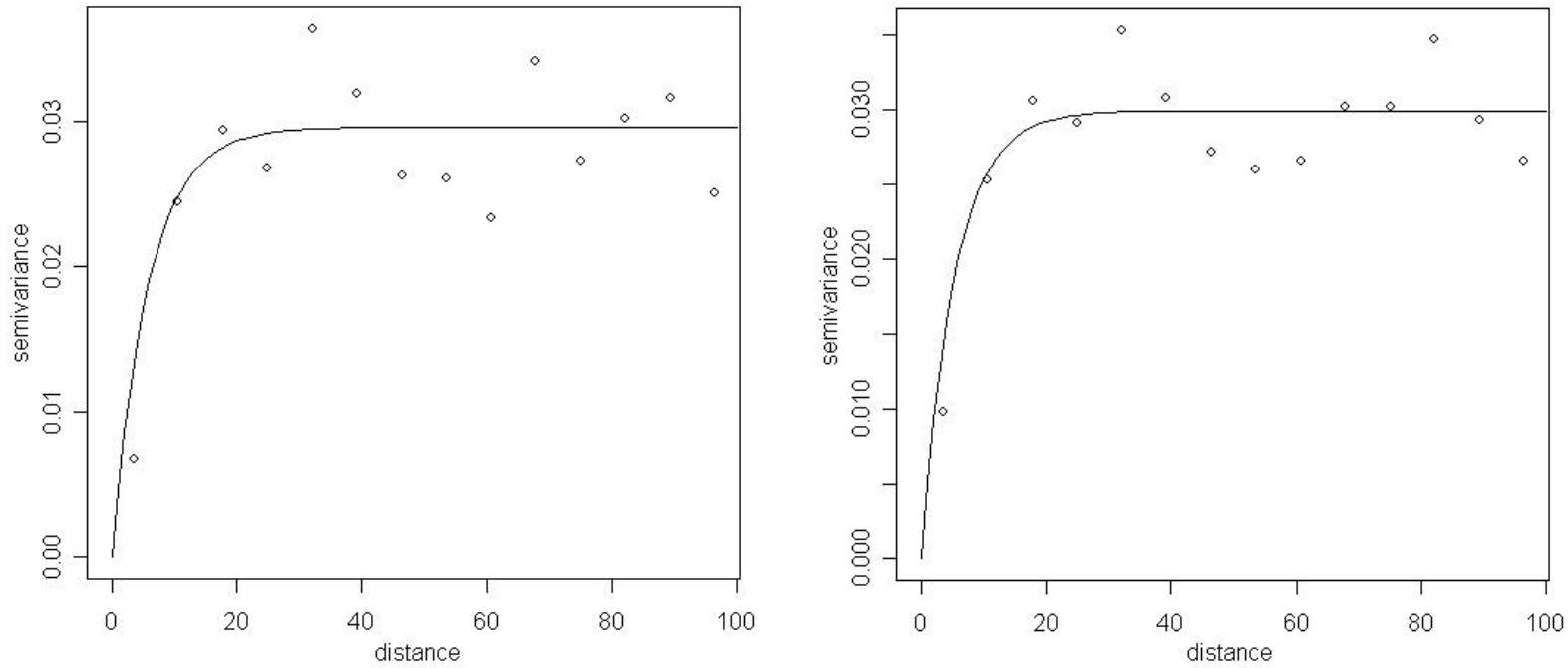

(a) East Tails (b) East and West Tails combined

Figure: The exponential variogram for the East Tails, combined East & West Tails.

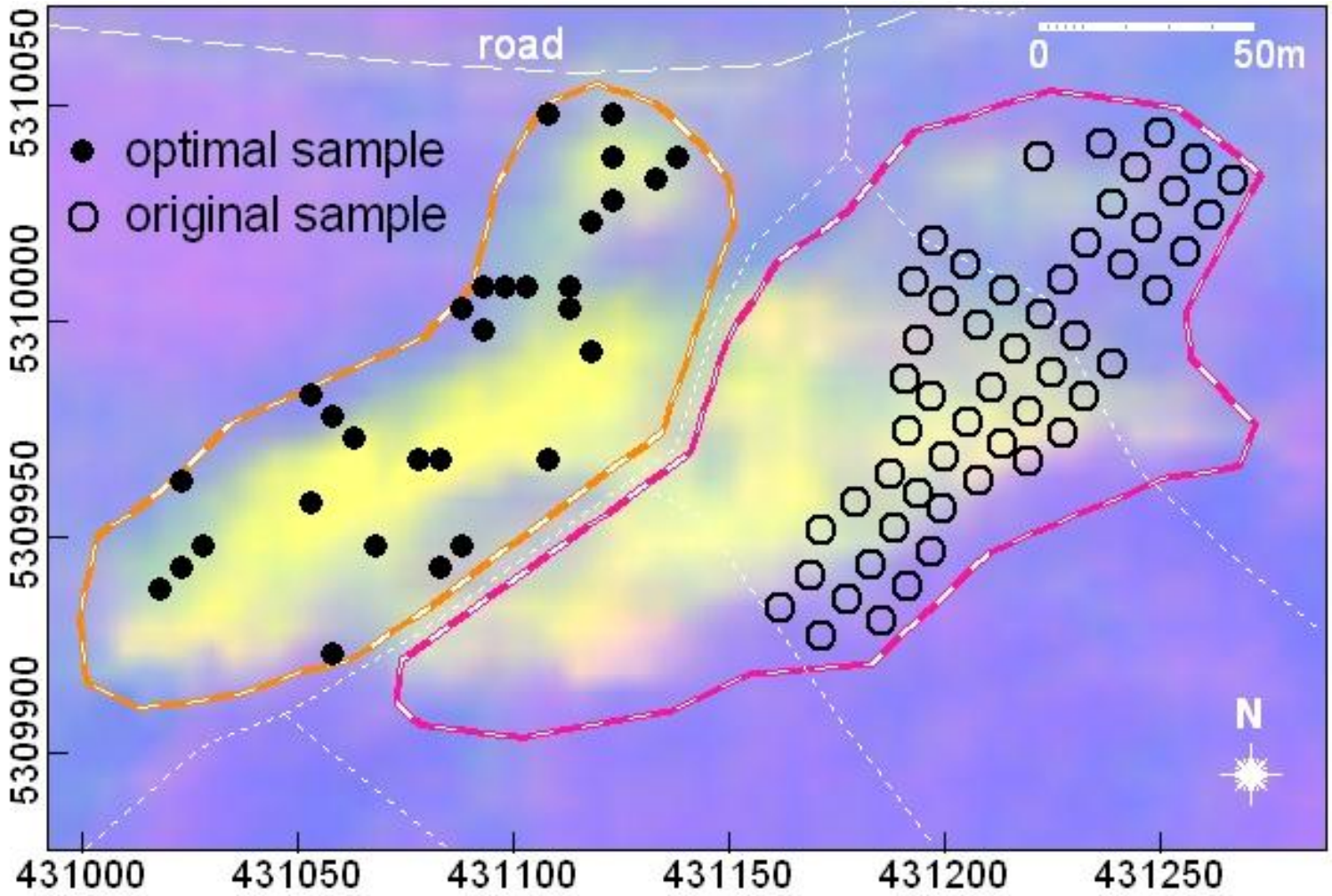

Figure: Prospective optimal sampling scheme in the West Tails using East Tails samples.

A prospective sampling scheme

- The optimal sampling scheme constructed using the kriging external drift variance approach are spread over the West Tails region while retaining some close pairs of samples.
- These close pair samples are to improve the estimation of the variogram model.
- The mean kriging with external drift variance for the West Tails, using the combined East and West Tails sampling data, is 6.8×10^{-4} for the West Tails.
- This mean kriging variance was approximately the same when either of the two variograms was used.
- The optimal sampling scheme resulted in a mean kriging with external drift variance for the West Tails of 3.3×10^{-4} using the variogram derived from the East Tails data.
- This indicates that the optimal sampling scheme contains samples that reduces the mean kriging with external drift variance for the previously designed grid sampling scheme in the West Tails.

What have we learnt?

- This study demonstrates that designing sampling schemes using simulated annealing results in much better selection of samples from an existing scheme in terms of prediction accuracy.
- The use of secondary information in designing optimal sampling schemes was also illustrated. Often these secondary information can be achieved at a relatively low cost and available over a greater region. These are the primary reasons for incorporating this information into the sampling design.
- Optimized sampling schemes using the mean kriging with external drift variance will result in sampling schemes that explicitly take into account the nature of spatial dependency of the data and together with hyperspectral data can be used to design sampling schemes in nearby unexplored areas.